



Review

Preparation of MnO₂-Carbon Materials and Their Applications in Photocatalytic Water Treatment

Kun Fan ¹, Qing Chen ^{1,2,*}, Jian Zhao ¹ and Yue Liu ¹¹ Chinese Research Academy of Environment Sciences, Beijing 100012, China² Ecological and Environmental Protection Company, China South-to-North Water Diversion Corporation Limited, Beijing 100036, China

* Correspondence: chenqing9821@163.com

Abstract: Water pollution is one of the most important problems in the field of environmental protection in the whole world, and organic pollution is a critical one for wastewater pollution problems. How to solve the problem effectively has triggered a common concern in the area of environmental protection nowadays. Around this problem, scientists have carried out a lot of research; due to the advantages of high efficiency, a lack of secondary pollution, and low cost, photocatalytic technology has attracted more and more attention. In the past, MnO₂ was seldom used in the field of water pollution treatment due to its easy agglomeration and low catalytic activity at low temperatures. With the development of carbon materials, it was found that the composite of carbon materials and MnO₂ could overcome the above defects, and the composite had good photocatalytic performance, and the research on the photocatalytic performance of MnO₂-carbon materials has gradually become a research hotspot in recent years. This review covers recent progress on MnO₂-carbon materials for photocatalytic water treatment. We focus on the preparation methods of MnO₂ and different kinds of carbon material composites and the application of composite materials in the removal of phenolic compounds, antibiotics, organic dyes, and heavy metal ions in water. Finally, we present our perspective on the challenges and future research directions of MnO₂-carbon materials in the field of environmental applications.

Keywords: water pollution; MnO₂-carbon materials; photocatalytic; environmental applications



Citation: Fan, K.; Chen, Q.; Zhao, J.; Liu, Y. Preparation of MnO₂-Carbon Materials and Their Applications in Photocatalytic Water Treatment. *Nanomaterials* **2023**, *13*, 541. <https://doi.org/10.3390/nano13030541>

Academic Editor: Diego Cazorla-Amorós

Received: 31 December 2022

Revised: 17 January 2023

Accepted: 23 January 2023

Published: 29 January 2023



Copyright: © 2023 by the authors. Licensee MDPI, Basel, Switzerland. This article is an open access article distributed under the terms and conditions of the Creative Commons Attribution (CC BY) license (<https://creativecommons.org/licenses/by/4.0/>).

1. Introduction

With the rapid development of modern industry and agriculture and the rapid growth of population, agricultural, industrial and domestic water use has increased tremendously [1,2]. Refractory toxic pollutants such as pesticides [3], antibiotics [4], textile dyes [5], and heavy metals [6,7] are discharged into water bodies, posing a huge threat to aquatic ecosystems and human health. Water pollution has become among the most pressing issues in the whole world [8]. Hence, green, highly efficient, and low-cost water treatment technologies are in urgent demand. Photocatalysis has been recognized as an ideal tool to eliminate recalcitrant contaminants in aqueous environments owing to its high efficiency, energy savings, low cost, environmental friendliness, lack of secondary pollution, and other characteristics [9–11].

Photocatalytic materials are the core of photocatalytic technology [2,12–14]. In recent years, semiconductors based on metal oxides are mostly used as photocatalysts for environmental remediation, such as MnO₂ [15], TiO₂ [16], ZnO [17], Fe₂O₃ [18], SnO₂ [19], etc. Photocatalytic reactions are initiated by absorbing light energy equal to or more than the bandgap of semiconductor photocatalysts, so the bandgap is an important parameter in defining the applicability of semiconductors in specific photocatalytic reactions [20,21]. Narrow bandgap semiconductors can improve the utilization of visible light, which is more beneficial for water purification applications [22]. Therefore, compared to wide-bandgap

semiconductor photocatalysts, narrow-bandgap manganese dioxide (MnO_2) can degrade organic pollutants under visible light irradiation [23,24]. In addition, MnO_2 is the most promising environment-friendly photocatalytic candidate material due to its low cost, non-toxic properties, ease of synthesis, rich structures and morphologies, outstanding adsorption, and oxidation capacity [25–27]. Cao and Steven [28] first validated its photocatalytic activity through the oxidation of 2-propanol in 1994. However, MnO_2 has low conductivity, the rate of charge transfer is slow, the photogenerated electron-hole pairs are prone to be recombined, and its efficiency as a photocatalyst is often restricted [29,30]. Meanwhile, the photocatalytic efficiency of MnO_2 is affected by its crystal form (α -, β -, γ -, δ -, and λ -types), morphology and structure. These factors are directly related to the preparation method, process, and parameters [31–35]. At present, a large number of studies have found that α - MnO_2 has good photocatalytic performance, and the catalytic efficiency can be further improved after MnO_2 and carbon are compounded [36–40]. MnO_2 has good compatibility with carbon materials, so many researchers combine MnO_2 with carbon materials to improve its photocatalytic efficiency [38,41–43].

Carbon-based materials are extensively used in water treatment as they are economical, abundant in nature, and environmentally friendly, and they show many advantages due to their excellent characteristics [44]. Carbon materials have a well-known electron-storage capacity, which can accept photon-excited electrons to promote charge separation and inhibit electron-hole pair recombination [43,45]. As adsorbents, carbon materials can offer a larger surface area and adsorb a large number of pollutants to the catalyst surface [46]. At the same time, as dopants and sensitizers, carbon materials can improve the solar absorbance range of MnO_2 to improve photocatalytic activity [47]. There is a good coupling effect between carbon materials and MnO_2 , so their composite has become an important field to be explored. Diverse types of MnO_2 -carbon composites have been investigated as photocatalysts to achieve better photocatalytic activity as well as more stable cycling performance. Many researchers have indicated that combining MnO_2 with carbon-based materials can diminish the recombination of charge carriers and enhance its photocatalytic performance [30,48–50].

Graphene [51], graphitic carbon nitride ($g\text{-C}_3\text{N}_4$) [52], carbon nanotubes (CNT) [53], carbon quantum dots (CQDs) [54], carbon fibers (CFs) [55], and other carbon materials have many unique properties like rich pore structure and active sites, high specific surface area, good electrical conductivity, excellent electron transport and adsorption ability, which are considered as the superior carriers or co-catalyst of semiconductor photocatalysts [56–59].

In recent years, multi-component composites based on MnO_2 and carbon materials have become a research hotspot in the application field of water treatment. There are many articles on the synthesis and application research of MnO_2 -carbon materials, but it is a big challenge to choose a suitable preparation process to make it more suitable for specific applications. We studied the photocatalytic degradation of organic compounds by MnO_2 -graphene. The photocatalytic efficiency of MnO_2 -graphene three-dimensional (3D) composites prepared by thermal reduction was as high as 92%. The primary goal of this review is to investigate the current application of MnO_2 -carbon materials for comprehensive adsorption and photocatalytic treatment of water. We summarize the preparation methods of different types of carbon materials combined with MnO_2 , then analyze the application development of MnO_2 -carbon composites in photocatalytic degradation of various refractory organic or inorganic pollutants in water, last, we discuss the existing problems and future prospects.

2. Preparation Methods of MnO_2 -Carbon Composites

2.1. Hydrothermal Method

The hydrothermal method with water as the reaction medium has become one of the common methods to prepare MnO_2 -carbon composites because of its economic simplicity and environmental protection [60–62]. Nanoparticles with different particle sizes, crystal forms, and morphologies can be obtained by adjusting hydrothermal conditions with high

reactivity, controllable conditions, and various synthesis types. In addition, the closed environment with high temperature and high pressure can effectively enhance the close contact between MnO_2 and carbon materials, improve the transmission speed of electrons, and improve the photocatalytic activity of the composite materials to some extent [63,64]. The hydrothermal method is widely used, which can prepare different dimensions and types of MnO_2 -carbon composites [65–75].

For example, Chhabra et al. [43] prepared α - MnO_2 -RGO nanocomposite by a facile hydrothermal method with RGO reduced by chemical reduction (Figure 1a). In the nanocomposite, the one-dimensional (1D) rod-shaped MnO_2 increases the flow of electrons in the longitudinal direction and reduces the possibility of electron-hole pair bonding. On the other hand, two-dimensional (2D) RGO nanosheets have a large surface area and pore volume, which can prevent charge recombination by aiding in the quick transport of the charges. With the introduction of RGO nanosheets, the surface area of the material increased to $87.159 \text{ m}^2\text{g}^{-1}$, and the composite photocatalyst exhibited efficient adsorptive photocatalytic performance. Wang et al. [76] prepared CNT- MnO_2 composite film by depositing MnO_2 nanosheets on CNT film using the hydrothermal method. Under different hydrothermal times, the coverage of MnO_2 on CNTs films will change. The optimized composite film can be folded into different sizes and shapes, exhibiting excellent flexibility and stability. Doping metal or non-metal on carbon materials or MnO_2 can incorporate the unique characteristics of different materials to improve performance [77–86]. Shan et al. [87] first prepared K and Na atom doped $g\text{-C}_3\text{N}_4$ via the thermal treatment of thiourea and KBr/NaBr , respectively, and then added them into KMnO_4 solution for hydrothermal reaction to synthesize K/Na doped $g\text{-C}_3\text{N}_4@/\text{MnO}_2$ composite. The MnO_2 nanosheets were vertically assembled on the surface of $g\text{-C}_3\text{N}_4$ with a stable structure and shortened the diffusion path lengths for electrons. Metal atoms intercalated into the $g\text{-C}_3\text{N}_4$ interlayers, which enhanced the conductivity, served as the charge transfer channel between adjacent layers to promote charge transfer and hinder the recombination of photogenerated carriers.

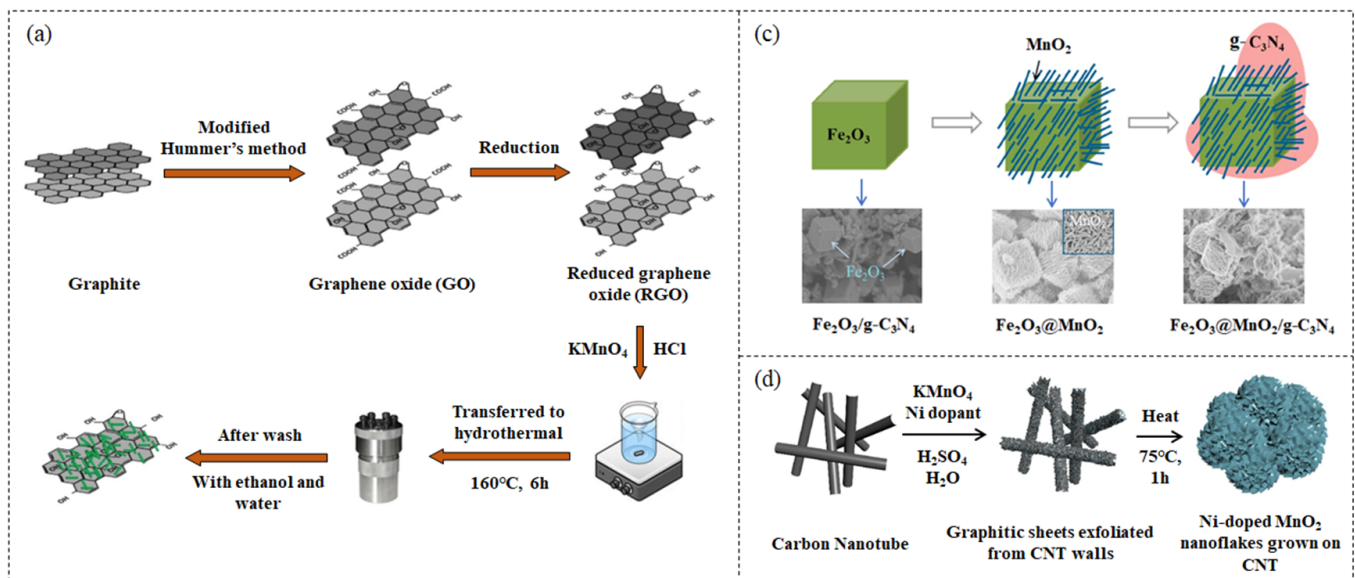


Figure 1. Cont.

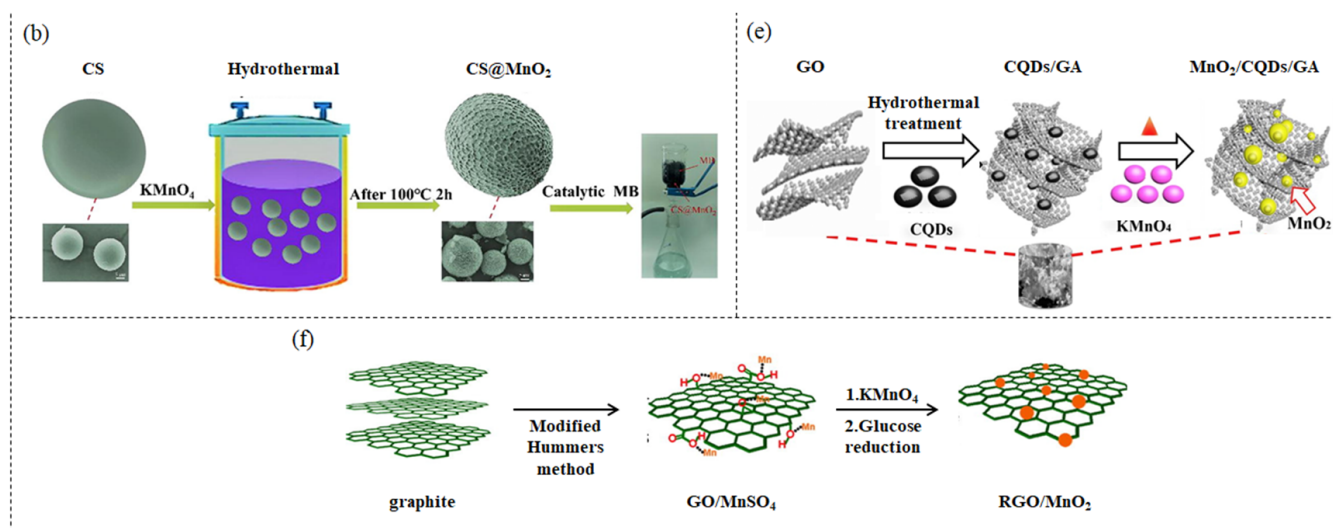


Figure 1. (a) Schematic illustration of the preparation of MnO_2 -RGO nanocomposite. Figures reprinted with permission from ref. [43]. Copyright 2019; Elsevier Ltd. (b) Schematic diagram of the procedure used to prepare carbon spheres@ MnO_2 . Figures reprinted with permission from ref. [88]. Copyright 2019; Elsevier Ltd. (c) Schematic illustration of the formation of Fe_2O_3 @ MnO_2 /g- C_3N_4 . Figures reprinted with permission from ref. [89]. Copyright 2020; Elsevier Ltd. (d) Schematic illustration of the growth mechanism of Ni-doped MnO_2 on CNT. Figures reprinted with permission from ref. [90]. Copyright 2018; Elsevier Ltd. (e) Schematic of the synthesis of RGO/ MnO_2 hybrids. Figures reprinted with permission from ref. [91]. Copyright 2014; Elsevier Ltd. (f) the fabrication procedure of the MnO_2 /CQDs/graphene composite aerogel. Figures reprinted with permission from ref. [92]. Copyright 2018; Elsevier Ltd.

In addition to 2D composites, nano-sized MnO_2 can be uniformly incorporated into the porous structure of 3D carbon materials via the hydrothermal method, thus improving the photocatalytic activity of hybrid catalysts [93–97]. Nui et al. [98] synthesized Graphene/nano α - MnO_2 hybrid aerogel in an isopropanol-water system via hydrothermal-reduction. The needlelike α - MnO_2 nanoparticles are covalently bonded with graphene without damaging the integrity of the graphene structure and are doped in the graphene aerogel uniformly. Due to the porous structure of the hybrid aerogel and the high dispersibility of the MnO_2 on graphene, the as-prepared composite exhibits good catalytic activity. Wan et al. [88] prepared flower-like core-shell MnO_2 -coated carbon aerogels via the hydrothermal method as a superior photocatalyst to remove organic dyes from an aqueous solution (Figure 1b). Dong et al. [99] prepared 3D MnO_2 /N-doped graphene hybrid aerogel by self-assembly. MnO_2 nanosheets and nanotubes were first synthesized by a double aging method and hydrothermal method, respectively, then N-doped graphene aerogels were created via hydrothermal-freeze drying process using ethylenediamine as the reductant and nitrogen source. The size and morphology of MnO_2 play an important role in tailoring the structures and properties of 3D graphene aerogels. The laminar structure of MnO_2 nanosheets with the graphene conductive substrate is beneficial to enhancing the charge transfer, shortening the diffusion pathway of pollutants, and affording more active sites. However, excessive MnO_2 nanosheets on graphene might aggregate and inactivate, which adversely affects the overall catalytic activity.

In order to further improve the properties of MnO_2 -carbon materials, many researchers also add green and economical polymers, oxides, or other carbon materials to the MnO_2 -carbon materials to prepare ternary composites, and the hydrothermal method is the most common preparation scheme [100–102]. For example, Iqbal et al. [103] prepared PANI@CNT/ MnO_2 ternary composite with rough interwoven fibrous and porous structure by the combination of hydrothermal methodology and in situ oxidative polymerization of aniline. The synergistic effect of the three enhances the specific surface area,

thermal and electrical conductivity, and provides channels for the transport of charge carriers, thus enhancing the performance of the material. Wang et al. [89] also utilized the α - Fe_2O_3 core/shell configuration to modify g- C_3N_4 , and prepared a dual Z-scheme α - Fe_2O_3 @ MnO_2 /g- C_3N_4 ternary composite by two-step hydrothermal method (Figure 1c). The Fe_2O_3 @ MnO_2 core/shell promoter modulates the electronic structure through the dual Z-scheme heterojunction, thus improving the separation efficiency of photo-generated electron-hole pairs. Due to its narrow bandgap, the composite material has a broad absorption in the visible light region, low cost and excellent performance, which is more conducive to practical application. Xu et al. [104] selected CC as the substrate for the growth of MnO_2 , coated RGO on the surface of CC, and synthesized CC/RGO/ MnO_2 composites by dipping method and hydrothermal method. CC/RGO can provide a large specific surface area as the skeleton, and the good conductivity of carbon materials can accelerate electron transfer, the resulting composite shows good photoelectrochemical activity. Li et al. [105] synthesized CNT/rGO@ MnO_2 particles through a hydrothermal reaction and then obtained a sandwich-like film with a 3D multilevel porous conductive structure via vacuum filtration and freeze-drying treatment. Nano-sized pores increase the specific surface area and provide a large number of active sites. MnO_2 grows in situ on the carbon skeleton, and the two are tightly connected, which facilitates electron transportation and enhances structural stability.

Solvothermal and microwave irradiation are improved methods of hydrothermal synthesis [61]. Among them, the solvothermal method is based on the same principle as the hydrothermal method. As water-sensitive compounds cannot be synthesized by the hydrothermal method, water can be replaced with an organic solvent to carry out the reaction [106–109]. For example, Asif et al. [90] synthesized an urchin-like morphology Ni-doped MnO_2 /CNT nanocomposites by a one-step solvothermal reaction (Figure 1d). Ni doping enhances the conductivity of MnO_2 and increases the surface area and cycle stability of the composite. Microwave irradiation heating reduces energy consumption compared to hydrothermal reactions, effectively shortens the synthesis time of complexes, and improves product homogeneity [110–112]. For example, Sivaraj et al. [110] reported a microwave-assisted process to synthesize the hybrid CNTs- MnO_2 nanocomposite. The dispersed MnO_2 nanospheres are uniformly attached to the CNTs' side walls, and a synergistic effect increases the light absorption range, promotes charge separation, and enhances stability.

2.2. In Situ Redox Deposition

Although hydrothermal self-assembly is economical and environmentally friendly, and widely used, it requires high temperature and pressure and a long reaction time, which is not suitable for large-scale production and applications [113]. In situ redox deposition is mild, simple, and suitable for the compounding of a wide range of metal oxides with carbon materials, which is another important method for the preparation of MnO_2 -carbon composites. It uses the carbon material as a substrate and involves the in situ deposition of MnO_2 nanostructures onto the surface of carbon materials through a redox reaction to form a nanocomposite, using the carbon material as a substrate, where the MnO_2 has uniformly and tightly adhered to the surface of the carbon material [114–125].

For example, Qu et al. [91] adopted the modified Hummers method and prepared a pristine GO/ MnSO_4 suspension, then the pristine suspension of GO/ MnSO_4 was in situ transformed into GO/ MnO_2 composites in combination with KMnO_4 , and finally further into RGO/ MnO_2 composites by means of glucose-reduction (Figure 1e). Singu et al. [126] synthesized CNTs- MnO_2 nanocomposites through the in situ reduction of KMnO_4 using MWCNTs as the reducing agent and supporting substrate. During the preparation process, the loading of MnO_2 can be adjusted by varying the amount of KMnO_4 , thereby optimizing the performance of the composite material. Wang et al. [127] adsorbed Mn^{2+} on the surface of g- C_3N_4 through the NH_2 groups in g- C_3N_4 for the first time, underwent a redox reaction with KMnO_4 , and synthesized a novel 2D MnO_2 /g- C_3N_4 heterojunction composite by in situ deposition of δ - MnO_2 . The bandgaps of MnO_2 and g- C_3N_4 synthesized have a wide

visible light response and light absorption range, which are 1.56 eV and 2.69 eV, respectively. At the same time, the matched band structures and the heterojunctions with solid (C-O) bonding between them interface promoted the transfer/separation of photogenerated charge carriers, enhanced the light-harvesting ability, thus the photocatalytic activity can be greatly enhanced. Peng et al. [128] also synthesized N-doped CNT (NCNT) by chemical vapor deposition, and deposited MnO₂ onto the NCNT surface using in situ oxidation to prepare MnO₂/NCNT composites. The synergistic effect of MnO₂ and NCNT obviously improved interfacial electron transfer, which can replace noble metals for the catalytic oxidation of organics.

In carbon materials, the existence of π - π interactions and van der Waals forces between the graphene nanosheets make it easy to aggregate and stack during processing, resulting in reduced surface areas and hidden active sites [129,130]. The quantitative loss of nanoscale materials during the recycling process may influence the fate of adsorbed contaminants, thus causing potential environmental risks [131]. The porous structure of composite films and aerogels can prevent the aggregation of nanosheets and afford more active sites for pollutant diffusion and oxidation. The structure is stable and easily recycled for reuse, which is a superior support for MnO₂ in the treatment of water, while in situ deposition of MnO₂ can also improve the mechanical and electron transport properties of carbon materials [132–137]. For example, Lv et al. [92] used 3D CQDs/graphene composite aerogels formed by the hydrothermal method as the reducing agent, which reacted with KMnO₄ to synthesize stable MnO₂/CQDs/graphene composite aerogel (Figure 1f). The 3D network structure avoided the reunion of the graphene nanosheets and the MnO₂ nanoparticles, and the CQDs served as a bridge for connecting MnO₂ and graphene, which effectively improved the conductivity and stability of the composite. Jyothibasudhan et al. [138] prepared cellulose/f-CNT/MnO₂ composite films via the direct redox deposition method to uniformly grow MnO₂ nanostructures on cellulose/functionalized CNT (f-CNT) conductive substrates. The synthetic procedure is simple, inexpensive, environmentally friendly, and can be synthesized in large-scale batches. The synthesized materials have unique porous structures, large specific surface areas, and excellent conductivities.

2.3. Electrochemical Deposition

Electrochemical deposition is an effective strategy for the synthesis of nanoscale materials and functionalized composites [106] and has been widely used in synthesizing carbon materials such as MnO₂-modified carbon cloth and graphene [139–146]. Zhang et al. [141] synthesized hierarchical MnO₂ nanostructures on activated carbon cloth via a high-voltage anodic electro-deposition process, and the activated carbon cloth substrate enhanced the conductivity and hydrophilicity of the material. Zhu et al. [147] synthesized PANI@ γ -MnO₂/CC ternary hybrid material via hydrothermal and in situ electrochemical polymerization (Figure 2a). The coating PANI layer with a 3D hierarchical structure provides a high specific surface area (96.3389 m²g⁻¹), which is higher than that PANI@ γ -MnO₂ (41.8632 m²g⁻¹) and CC(21.1902 m²g⁻¹) and accelerates the ion diffusion and electron transfer. Li et al. [148] synthesized mesoporous MnO₂ with high density pores on carbon aerogels substrate by electrochemical deposition. Mesoporous materials can increase the active sites and enhance the electric conductivity, which is more conducive to the transport of electrons and ions. In photocatalytic applications, they can effectively prevent the recombination of photogenerated electrons and holes to improve photocatalytic activity. At the same time, the obtained MnO₂/carbon aerogel composites are green, low-cost and good in cycle stability, which have potential research and application value.

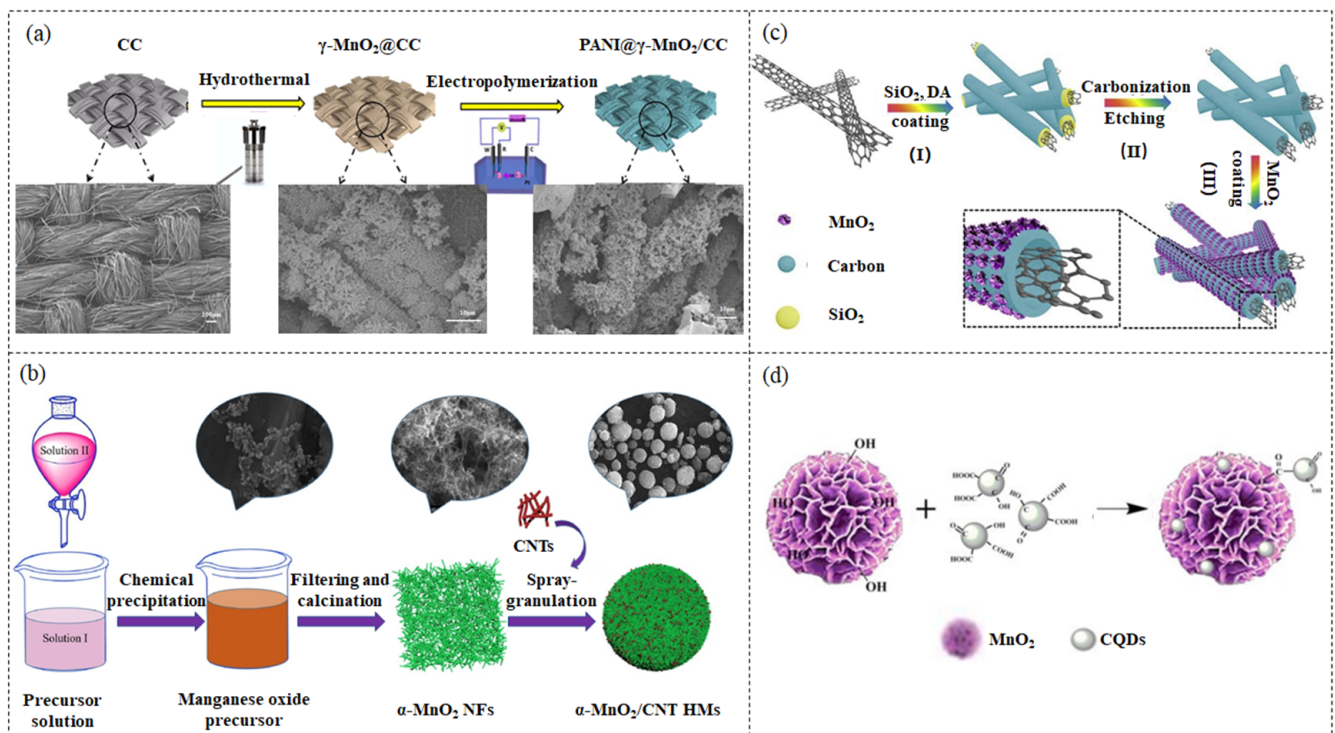


Figure 2. (a) The schematic diagram of the process of preparing ternary composite PANI@ γ -MnO₂/CC composite materials and SEM images of different materials. Figures reprinted with permission from ref. [147]. Copyright 2022; Elsevier Ltd. (b) Schematic illustration of the preparation of α -MnO₂/CNT HMs and SEM images at different synthetic stages. Figures reprinted with permission from ref. [149]. Copyright 2019; Elsevier Ltd. (c) Schematic illustration of the fabrication of CNT@NCT/MnO₂ composites. (I) CNTs were sequentially coated with a thick SiO₂ layer and carbon layer; (II) the removal of the SiO₂ layer; (III) the growth of ultrathin MnO₂ nanoflowers on the carbon layer. Figures reprinted with permission from ref. [150]. Copyright 2019; Elsevier Ltd. (d) Schematic representation of the preparation of CQDs/MnO₂ nanoflowers. Figures reprinted with permission from ref. [151]. Copyright 2017; Electrochemical Society.

2.4. Co-Precipitating Method

The chemical co-precipitation method is a simple process, with low calcination temperatures and good homogeneity of the prepared complexes, and is one of the common methods for the preparation of carbon composites at low temperatures [64,152–154]. Zeng et al. [155] synthesized 1D α -MnO₂ nanowires and 2D GO nanowires to prepare α -MnO₂/GO nanohybrids by mechanical grinding and co-precipitating method. The sub-micron GO sheets can occupy the interspace of the interconnected network of α -MnO₂ nanowires so that the two can be better combined. By comparing the materials prepared by the two methods, it can be found that the co-precipitating method is more conducive to the tight binding of MnO₂ and GO and facilitates heat and electron transfer between these two materials. However, mechanical grinding may destroy the layered structure of GO and produce more defects, which is not conducive to photon absorption and electron transfer. Liu et al. [149] first synthesized α -MnO₂ nanofibres/carbon nanotubes hierarchically assembled microspheres (α -MnO₂/CNT HMs) via a facile chemical precipitation/spray-granulation combined methodology (Figure 2b). The α -MnO₂ NFs were homogeneously anchored on a highly conductive CNTs framework, forming a close-packed network structure, which remarkably improved the electron-transfer capability. The composite material has excellent stability and cycling durability, low cost, and wide application prospects. Kumar et al. [156] prepared an Ag-doped MnO₂-CNT nanocomposite using a co-precipitation route. The spheroidal-shaped Ag nanoparticles covered the

CNT surface, and its high surface area to volume ratio provides a large number of active sites, showing excellent adsorption performance. Xia et al. [157] grew MnO₂ nanosheets in situ on the surface of exfoliated g-C₃N₄ nanosheets by a wet-chemical method, forming a 2D/2D g-C₃N₄/MnO₂ heterojunction. The photoinduced electrons in MnO₂ can combine with the holes in g-C₃N₄ to enhance the extraction and utilization of photo-generated carriers and improve the degradation rate of pollutants.

2.5. Template Method

The template method is mostly used for the preparation of 3D composites [158,159]. Le et al. [160] used diatomite as a template for the massive production of 3D porous graphene by the chemical vapor deposition method. After removing the template, the 3D graphene was N-doped by a hydrothermal reaction, and then the N-doped 3D porous graphene@MnO₂ hybrid structure was obtained by deposition of MnO₂ nanosheets. The MnO₂ nanosheets with a brushy structure were uniformly deposited on the surface of porous graphene, and the synergistic interactions between them enhanced the stability of the composite. After removing the diatomite, the composite retained the 3D structure and surface features of the diatomite template. Moreover, the abundant edges and defects formed during the template removal process and defects caused by nitrogen doping improve the conductivity and charge transfer rate of the composite. The MnO₂ nanosheets with a brushy structure were uniformly deposited on the surface of porous graphene, and the synergistic interactions between them enhanced the stability of the composite. Wang et al. [150] fabricated 3D CNT@NCNT@MnO₂ composites with unique tube-in-tube nanostructures through the sacrificial template method (Figure 2c). The composite has an N-doped 3D double-carbon layers hollow structure and attaches tightly with MnO₂ nanoflowers grown on its surface, exhibiting large pores, high conductivity, large specific surface areas, and fast diffusion of electrons. Shan et al. [161] also prepared C-doped g-C₃N₄ (CCN) using polyporous melamine foam (MRF) as a template and then exploited the synergistic advantages of 2D architectures, coupled CCN with MnO₂ nanosheets by a hydrothermal method to prepare efficient CCN@MnO₂ composite. The doping of carbon promoted electron transfer, and the MRF template can prevent the aggregation of sulfourea crystals, thereby reducing the thickness of CCN nanosheets and increasing the specific surface area (40.2 m²g⁻¹).

2.6. Ultrasonic-Assisted and Sonochemical Methods

The Sonochemical-assisted uses sound energy to agitate the composite solution, causing it to undergo a physical or chemical transformation [162]. It can prevent material stacking, enlarge the interlayer spacing of carbon materials such as graphene, facilitate uniform loading of MnO₂ and enhance the photocatalytic properties of the synthesized semiconductors [64,106]. As a result, it is widely used to prepare various MnO₂-carbon nanocomposites [163–169]. Chai et al. [170] synthesized S,O co-doped graphite, carbonitride quantum dots (S, O-CNQDs) by a solid-state reaction method, and in situ synthesized MnO₂ nanosheets in S,O-CNQDs dispersion solution to prepare MnO₂-S,O-CNQDs nanocomposite with the ultrasonic-assisted. The as-prepared composite material has uniform size and good dispersion, which is a promising nanomaterial. Xu et al. [151] synthesized the CQDs/MnO₂ nanoflowers through the sonochemical method (Figure 2d), which has a high specific surface area (168.8 m²g⁻¹) and excellent cycle stability. CQDs were uniformly distributed on the transparent petals of δ-MnO₂, which improved the conductivity of MnO₂ nanoflowers and provided a large number of functional groups and active sites.

2.7. Other Methods

Many other novel options are also used to prepare MnO₂-carbon materials [171–173]. For example, Jia et al. [174] prepared CNTs/MnO₂ composites by in situ synthesis of CNTs on MnO₂ nanosheets using the hydrothermal method and the chemical vapor deposition method. The vertically aligned MnO₂ nanosheets shortened the ion diffusion path, the

in situ formed CNTs improved the electrical conductivity and structural stability, and the hierarchical porous structure increased the specific surface area ($20.4 \text{ m}^2\text{g}^{-1}$ to $38.2 \text{ m}^2\text{g}^{-1}$) and active sites. Abdullah et al. [175] used polyacrylonitrile (PAN) as a carbon precursor to prepare nanofibers (NFs) by an electrospinning process and incorporated MnO_2 nanoparticles into ACNFs to prepare composite activated carbon nanofibers (ACNFs/ MnO_2) by carbonization and activation. The incorporation of MnO_2 increased the specific surface area (478.2 to $599.4 \text{ m}^2\text{g}^{-1}$), pore size ($0.285 \text{ cm}^3\text{g}^{-1}$), and total pore volume ($0.299 \text{ cm}^3\text{g}^{-1}$) of the composite material. Wei et al. [176] prepared MnO_2 /3D graphene composites by the reverse microemulsion method. In this reaction, the graphene substrate was used as a sacrificial reductant to undergo a redox reaction with KMnO_4 to grow MnO_2 in situ on 3D graphene, and the MnO_2 mass loading of the composite was controlled by changing the ultrasonication time in the in situ growth process. Nanoscale MnO_2 layers were uniformly coated on the internal surface of 3D graphene, and the continuous 3D interpenetrating microstructures prevented the restacking of graphene sheets. Zhu et al. [177] prepared free-standing 3D graphene/ MnO_2 hybrids by depositing MnO_2 nanosheets onto a 3D graphene framework through a solution-phase assembly process. Unlike 1D MnO_2 , the flower-like architecture of deposited MnO_2 nanosheets have a larger specific surface area and are uniformly anchored on a 3D graphene framework with strong adhesion, there is a strong interaction between them, so the prepared hybrids showed good mechanical properties. Pang et al. [178] proposed a simple room-temperature water bath method to deposit crystalline MnO_2 on CNTs to prepare CNT- MnO_2 nanocomposites. This scheme can control the phases and morphologies of the composite products by changing the pH of the reaction solution. Wang et al. [179] assembled GO, MnO_x , and polymer carbon nitride (CN) into free-standing GO/ MnO_x /CN ternary composite film by employing the vacuum filtration method. The prepared composite film has good stability, mechanical property, and recyclability and is more suitable for the practical application of photocatalysis.

To sum up, MnO_2 -carbon composites can be prepared and modified in various ways, and the finally obtained multifunctional materials have great application potential in water treatment. Each preparation method has its own unique advantages, and the fabrication of specific nanocomposites can be improved by selecting the most suitable preparation method, which can be used to treat various types of sewage treatment to different pollutants (Table 1).

Table 1. Summary of preparation methods, products, and morphological characteristics of synthesizing MnO_2 -carbon materials.

MnO_2	Carbon Material	Synthesis Method	Composite Product	Morphology	Ref.
ultrafine MnO_2 nanowires	CC	hydrothermal	MnO_2 @CC	Weedy 1D ultrafine MnO_2 nanowire interconnection network covered on the surface of CC.	[74]
MnO_2	g- C_3N_4	In situ redox deposition	MnO_2 /g- C_3N_4	flower-like MnO_2 nanosheets deposited on g- C_3N_4 , resulting in surface roughness.	[125]
MnO_2	3D Graphene Networks	Electrochemical deposition	3D Graphene/ MnO_2	MnO_2 nanoporous structures were uniformly coated on a 3D graphene network skeleton.	[146]
α - MnO_2	HMCNTs	Co-precipitating	MnO_2 /HMCNTs	MnO_2 was deposited on the surface of CNTs and provided active sites.	[154]

Table 1. Cont.

MnO ₂	Carbon Material	Synthesis Method	Composite Product	Morphology	Ref.
MnO ₂	g-C ₃ N ₄	Sonochemical	g-C ₃ N ₄ /MnO ₂	Different sizes of materials were obtained by ultrasound with different amplitudes.	[169]
MnO ₂ Polyhedron Precursors	Bulk-g-C ₃ N ₄ nanosheets	Calcination	3D/2D MnO ₂ /g-C ₃ N ₄ Nanocomposite	MnO ₂ was wrapped by the g-C ₃ N ₄ layers.	[171]
MnO ₂ Nanorods	Mn-modified alkalized g-C ₃ N ₄	Impregnation	Z-scheme MnO ₂ /Mn-modified alkalized g-C ₃ N ₄ heterojunction	In the process of Mn modifying alkalized g-C ₃ N ₄ , slender rod-shaped MnO ₂ was formed.	[172]
layered MnO _x	GO	hydrothermal	GO/MnO _x composites	nanosheets	[75]
α-MnO ₂ nanorods	MWCNTs	direct pyrolysis	MWCNTs/MnO ₂ nanocomposite	MnO ₂ nanorods are uniformly attached to the surface of MWCNTs.	[173]

3. Applications of Photocatalytic Technology in Water Treatment

With the growth of population and continuous development of industry and agriculture, the problem of water pollution has become increasingly prominent [180–182]. Various organic and inorganic pollutants have been detected in surface, ground, sewage, and drinking waters [183,184]. Among them, the pollutants (phenols, antibiotics, organic dyes, heavy metal, etc.) produced by agriculture [185], aquaculture [186,187], carbon aerogels, textiles [188,189] and other industries are highly toxic and difficult to biodegrade [180]. The pollution of water bodies will not only destroy the ecosystem but also seriously threaten human health [190,191]. These stubborn compounds have become important contaminants in water that need to be removed urgently. As common green materials, MnO₂ and carbon materials can use solar energy to degrade many types of pollutants, and the photocatalytic process is economical and environmentally friendly [192]. Therefore, the combination of the two has momentous research potential and application prospects in the field of photocatalytic water treatment, and the photocatalytic degradation of various pollutants by MnO₂-carbon materials has also been widely studied [193].

3.1. Phenolic Wastewater

Phenolic compounds are typical aromatic organic compounds that exist in sewage discharged from petroleum refineries, manufacturing of paints, pulp and paper manufacturing plants, and other industries [194–196]. At the same time, they are also a kind of important organic raw materials in the field of agricultural production and are widely used in the manufacture of pesticides, insecticides, and herbicides [197–199]. Their wide use in industry and agriculture makes them a large number of residues in the environment and a common organic pollutant in water, which have potential carcinogenicity, teratogenicity, and mutagenicity, with wide source, great harm and refractory degradation [200–202]. Among them, phenol and its derivatives (such as bisphenol A, chlorophenol, nitrophenol, etc.) are common phenolic pollutants in the water environment, which are highly toxic and cause serious pollution even at low concentrations [194,203–206]. Compared with other organic substances, they have a great impact on the environment.

Phenolic compounds usually have one or more hydroxyl groups attached to the aromatic ring [194]. In the photocatalytic process, hydroxyl radicals attack the cyclic carbon to produce various oxidation intermediates (such as hydroquinone, catechol, p-benzoquinone, etc.) [195]. These organic compounds are less harmful than the parent compounds and will eventually be photomineralized to carbon dioxide (CO₂), so as to achieve the purpose of

degradation [207]. Table 2 summarizes the progress in the photocatalytic degradation of phenolic compounds by various MnO₂-carbon materials. For example, Mehta et al. [207] prepared MnO₂@CQDs nanocomposites with a bandgap of 1.3 eV by a one-step hydrothermal method, which was used to degrade phenol under visible light. The spherical CQDs were deposited on the surface of MnO₂ nanorods, and the nanocomposite had a high specific surface area (95.3 m²g⁻¹). The optimal operating parameters were obtained after optimization under different reaction conditions, and after 50 min of visible light irradiation, the degradation rate of phenol reached 90%. The degradation rate was basically unchanged after three consecutive cycles, and the degradation rate can still reach 80% after five cycles, which the stability is good. Xia et al. [157] synthesized g-C₃N₄/MnO₂ heterostructured photocatalyst via in situ growth of MnO₂ nanosheets on the surface of exfoliated g-C₃N₄ nanosheets using a wet-chemical method. MnO₂ nanosheets and the g-C₃N₄ layers are closely combined, and the 2D layered structure can provide abundant active sites and shorten the transport distance of photogenerated charge carriers. Under the irradiation of xenon lamps, the ability of the composite material to degrade phenol is significantly increased, and it has good durability. Preparing the photocatalyst of the MnO₂-carbon composites with low bandgap can make full use of solar energy and provide a sustainable green approach for photocatalytic water treatment, and its application potential needs to be further developed [208–212].

Table 2. Study on MnO₂-carbon materials for photocatalytic degradation of phenolic compounds in aqueous solution.

Photocatalyst	Target Pollutant	Light Source	Photocatalyst Amount	Initial Concentration	Activity	Ref.
Titanium dioxide-manganese oxide/multi-walled CNT (TiO ₂ -MnO ₂ /MWCNT)	phenol	UV light 150 W fluorescent lamp	90 mg	300 mL 100 mg/L	40 min 100%	[208]
CQDs decorated MnO ₂ nanorods (MnO ₂ @CQDs)	phenol	visible light	/	100 mg/L	50 min 90%	[207]
MnO ₂ /g-C ₃ N ₄ (MG3)	phenol	visible light	50 mg	100 mL 5 mg/L	100 min 98%	[209]
2D g-C ₃ N ₄ /MnO ₂ heterojunctions (2D g-C ₃ N ₄ /MnO ₂)	phenol	visible light 300 W Xenon lamp	50 mg	50 mL 50 mg/L	180 min 73.6%	[157]
2D/1D protonated g-C ₃ N ₄ /α-MnO ₂ (CNM)	phenol	visible light 300 W Xe arc lamp	40 mg	80 mL 10 mg/L	120 min 93.8%	[67]
g-C ₃ N ₄ /MnO ₂ /Pt	Phenol; Bisphenol A	Solar source 300 W Xenon lamp	50 mg 20 mg PMS	100 mL 20 mg/L	30 min 20%→57%; 13%→97%	[210]
Dye-loaded MnO ₂ and chlorine-intercalated g-C ₃ N ₄ (MO/CN-Cl)	Phenol; 2,4- dichlorophenol	visible light 150 W Xe lamp	200 mg	50 mL 20 mg/L	1 h 47%; 1 h 60%	[211]
Graphene oxide/MnO ₂ nanocomposite (rGO/MnO ₂)	2-naphthols	visible light 20 W LED	100 mg	144 mg	12 h 97.2%	[193]
3 wt% MnO ₂ modified exfoliated porous g-C ₃ N ₄ nanosheet (GM3)	aromatic alcohols	visible light 150 W xenon lamp	/	20 mL 100 mg/L	80 min 78%	[212]

3.2. Antibiotic Wastewater

Antibiotics can prevent and treat a variety of bacterial infections in humans and animals and are widely used for human beings, animal husbandry, and aquaculture industries [213–215]. However, the overuse of antibiotics has imposed severe water environment problems [215]. According to statistics, approximately 60–90% of antibiotics cannot be completely metabolized by the human or animal body and will be excreted through feces [216–219]. These wastes may be dumped directly into wastewater or enter farmland as fertilizer and enter nearby water bodies through rainfall and irrigation [220,221]. Due to the poor biodegradability of most antibiotics, the sustained use of antibiotics makes them stay in the water for a long time, which may generate antibiotic-resistant genes (ARGs) and antibiotic-resistant bacteria (ARBs), resulting in increased microbial resistance, which poses a potential threat to human health and ecological systems [222–224]. Therefore, the degradation of antibiotics in water is an important and urgent task.

It has been reported that sunlight-driven photocatalytic technology can effectively remove antibiotics from water, among which the visible light-responsive MnO₂-carbon composite photocatalyst has great practical application potential [225,226]. We selected and listed the photocatalytic degradation rates of different types of antibiotics using MnO₂-carbon as a photocatalyst (Table 3). Du et al. [227] synthesized g-C₃N₄/MnO₂/GO heterojunction photocatalyst by wet-chemical method (Figure 3a). Composites with different ratios of g-C₃N₄, MnO₂, and GO have different catalytic activities, and the composites, after optimization, can degrade 91.4% of TC at most after 60 min of visible light irradiation. The TC removal rate only decreases by 10% after four cycles, and the sample structure has no change (Figure 3b–d). Excellent stability is more conducive to the practical application of photocatalysis. Liu et al. [228] synthesized the pumice-supported reduced graphene oxide and MnO₂ (PS@rGO@MnO₂) as a solid photocatalyst by a two-step hydrothermal method, which can effectively degrade 80% ciprofloxacin within 6 h under simulated sunlight, and the performance was not obviously decreased after three cycles, and all characteristic peaks remained intact, which proved its excellent reusability. In addition, the catalytic performance of PS@rGO@MnO₂ solid photocatalyst under actual sunlight is comparable to that under simulated sunlight, it has good removal performance for ciprofloxacin in actual natural water, and it can also degrade other antibiotics in water, which has great potential in the treatment of drinking water and surface water.

Table 3. Study on MnO₂-carbon materials for photocatalytic degradation of antibiotic in aqueous solution.

Photocatalyst	Target Pollutant	Light Source	Photocatalyst Amount	Initial Concentration	Activity	Ref.
Porous Z-scheme MnO ₂ /Mn-modified alkalized g-C ₃ N ₄ heterojunction (MnO ₂ /CNK-OH-Mn ₁₅ %)	tetracycline	visible light 300 W Xe lamp	50 mg	100 mL 10 mg/L	120 min 96.7%	[172]
Carbon nanosheet/MnO ₂ /BiOCl (Cs/Mn/Bi-1/1)	tetracycline hydrochloride	UV light 300 W mercury lamp	20 mg	100 mL 20 mg/L	30 min 80%	[225]
g-C ₃ N ₄ /diatomite/MnO ₂	tetracycline hydrochloride	visible light	30 mg	100 mL 50 mg/L	60 min 87%	[226]
g-C ₃ N ₄ /MnO ₂ /GO (CMG-10)	tetracycline hydrochloride	visible light 300 W xenon lamp	50 mg	100 mL 10 mg/L	60 min 91.4%	[227]

Table 3. Cont.

Photocatalyst	Target Pollutant	Light Source	Photocatalyst Amount	Initial Concentration	Activity	Ref.
$g\text{-C}_3\text{N}_4\text{-MnO}_2$ (CMn ₂)	tetracycline hydrochloride	visible light LED	30 mg	75 mL 20 mg/L	135 min 92.47%	[169]
Pumice-loaded rGO@MnO ₂ PS@rGO@MnO ₂	ciprofloxacin	sunlight 300 W xenon lamp	300 mg	30 mL 5 mg/L	6 h 80%	[228]
$g\text{-C}_3\text{N}_4/\text{MnO}_2/\text{Pt}$	sulfadiazine	Solar source 300 W Xenon lamp	50 mg 20 mg PMS	100 mL 20 mg/L	30 min 11%→68%	[210]

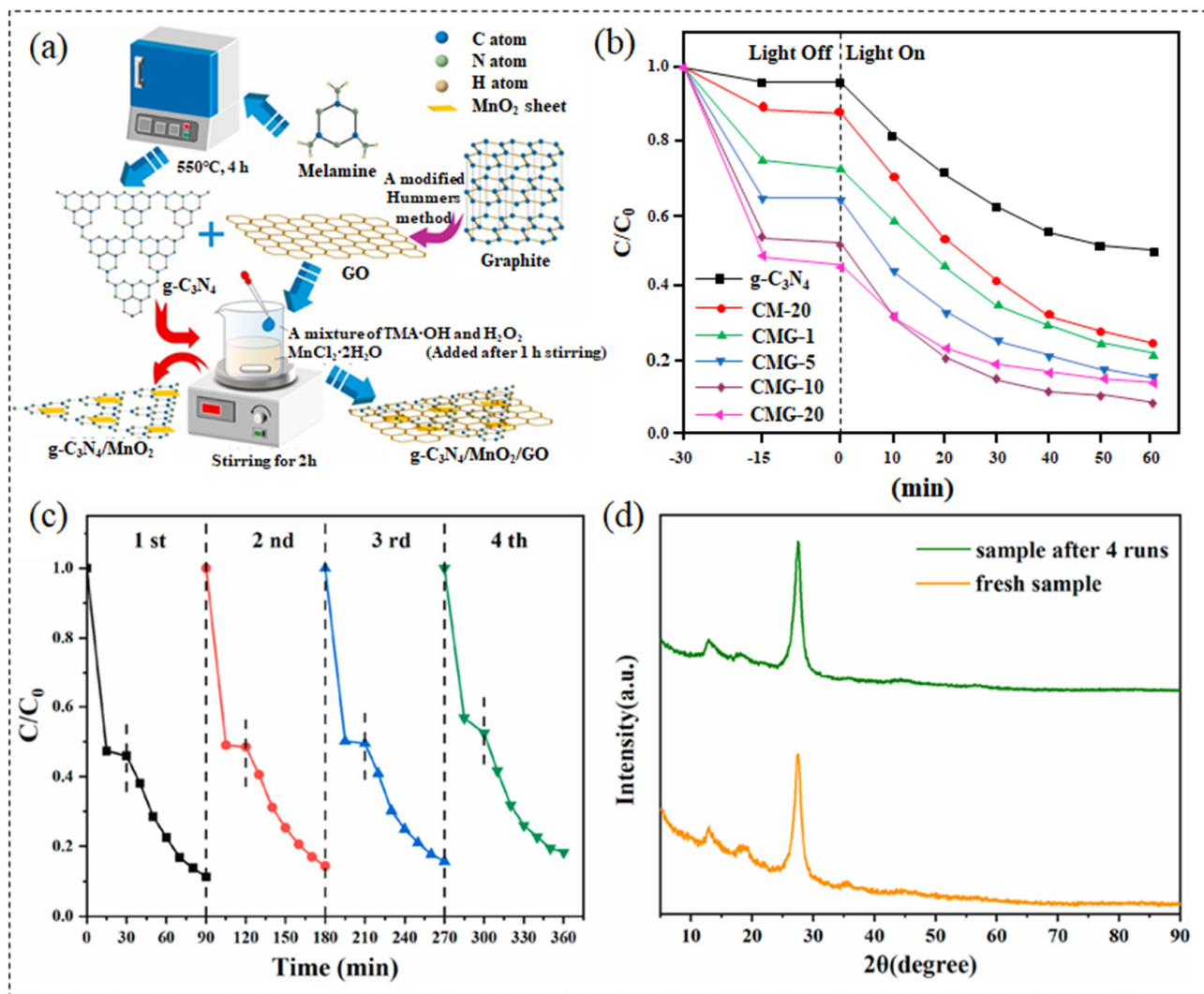


Figure 3. (a) Preparation process scheme; (b) Photocatalytic degradation rate under the visible light irradiation; (c) Recycle experiments for the degradation of TC and (d) XRD patterns before and after four runs of CMG-10. Figures reprinted with permission from ref. [227]. Copyright 2021; Elsevier Ltd.

3.3. Dye Wastewater

Dyes can impart or alter the color of a substance, which are widely used in a wide variety of industries, including textile, printing, leather, agriculture, pharmaceutical, and food industries [229–232]. According to statistics, more than 7×10^5 tons of dyes are produced annually worldwide, and about 15% of dyes will enter the environment with the

loss of wastewater during manufacturing and application processes [233,234]. The dyes have a complex structure, high biological toxicity, and are easily soluble in water but have poor biodegradability, which may accumulate in the water environment [132,235]. The colored dyes in the water will affect the transparency of water bodies, absorb and reflect sunlight entering the water, hinder the photosynthesis of aquatic plants and abolish the ecological balance of the water body [230,236]. In addition, its potential carcinogenicity, teratogenicity, and mutagenicity will also cause negative effects on human health [237,238].

Photocatalytic technology has the remarkable ability to degrade and decolorize organic dyes. In environment-cleaning applications, different kinds of semiconductor compounds play an important role in the photocatalytic removal of dyes [229]. In recent years, MnO₂-carbon materials have shown excellent performances in the photocatalytic degradation of organic dyes, which has attracted extensive research by researchers [239–249] (Table 4). Park et al. [250] synthesized PANI-rGO-MnO₂ ternary composites by polymerizing aniline with rGO and incorporating MnO₂. PANI can act as an excellent electron donor and hole conductor, as channels for electron transport and storage, and is a suitable substrate for visible light-responsive photocatalysts. The ternary heterostructure reduced the recombination of photogenerated electron-hole pairs and extended the light absorption range. The composites showed excellent photocatalytic activity, and 90% of methylene blue (MB) could be degraded under visible light irradiation within 2 h (Figure 4). Panimalar et al. [251] constructed the MnO₂/g-C₃N₄ heterostructure, which showed higher photocatalytic activity than pristine MnO₂ and g-C₃N₄ after 100 min of visible light irradiation. The degradation rate of MO could reach 92%. After five cycles, the composite photocatalyst was not obviously inactivated, showing high stability. This sort of material could be used as a photocatalytic practical device for wastewater treatment.

Table 4. Study on MnO₂-carbon materials for photocatalytic degradation of organic dye in aqueous solution.

Photocatalyst	Target Pollutant	Light Source	Photocatalyst Amount	Initial Concentration	Activity	Ref.
MnO ₂ /CNT	MB	visible light solar radiation	20 mg	50 mL 20 mg/L	75 min 70%	[239]
Cu-doped MnO ₂ /r-GO	MB	visible light 200 W tungsten bulb	20 mg	50 mL 5 mg/L	90 min 86.69%	[240]
PANI-rGO-MnO ₂	MB	visible light 150 W halogen bulb with Halogen cold light source	10 mg	5 mg/L	120 min 91%	[250]
MnO ₂ /BC	MB	27 °C sunlight 45 °C	10 mg	10 mL 10 mg/L	120 min 85% 97%	[241]
α-MnO ₂ nanowire/activated carbon hollow fibers (MnO ₂ @ACHF)	MB	visible light	20 mg	33 mg/L	240 min 99.8%	[38]
poly(3,4- ethylenedioxythiophene)/ GO/MnO ₂ (PEDOT/GO/MnO ₂)	MB	UV light sunlight	20 mg	50 mL	7 h 97.1% 7 h 98.9%	[242]
graphene nano sheets/CNT/MnO ₂ (GNS/CNT/MnO ₂)	MB MG	visible light 400 W metal Philips lamp	60 mg	250 mL 60 mg/L	60 min 71% 60 min 89%	[243]
GO@Fe ₃ O ₄ -MnO ₂	MG tartrazine	sunlight	10 mg	50 mL 10 mg/L	70 min 99.9% 80 min 98%	[244]

Table 4. Cont.

Photocatalyst	Target Pollutant	Light Source	Photocatalyst Amount	Initial Concentration	Activity	Ref.
Carbon nanosheet/MnO ₂ /BiOCl (Cs/Mn/Bi-1/1)	RhB MB	UV light 300 W mercury lamp	10 mg	100 mL 10 mg/L	25 min 97% 40 min 98%	[225]
g-C ₃ N ₄ /diatomite/MnO ₂	RhB	visible light	30 mg	100 mL 10 mg/L	50 min 94%	[245]
2D/1D protonated g-C ₃ N ₄ /α-MnO ₂ (CNM)	RhB	visible light 300 W Xe arc lamp	40 mg	80 mL 10 mg/L	60 min 98.8%	[67]
2D g-C ₃ N ₄ /MnO ₂	RhB	visible light 300 W Xenon lamp	50 mg	50 mL 10 mg/L	60 min 91.3%	[157]
MnO ₂ @GO (MG _{0.4})	RhB	visible light 500 W xenon–mercury lamp	40 mg	50 mL 20 mg/L	65 min 93.86%	[246]
g-C ₃ N ₄ /MnO ₂ (GCN/MnO ₂)	RhB	sunlight	4 mg	20 mL 9.6 mg/L	90 min 100%	[247]
Boron-doped carbon nitrides/MnO ₂ (BCN/MnO ₂)	RhB	visible light	25 mg	50 mL 10 mg/L	180 min 61.1%	[248]
g-C ₃ N ₄ /MnO ₂ /Pt	RhB MO	Solar source 300 W Xenon lamp	50 mg 20 mg PMS	100 mL 20 mg/L	30 min 99% 30 min 97%	[210]
nitrogen-doped graphene/MnO ₂ NG-MnO ₂	MO	visible light	5 mg	5 mL 20 mg/L	70 min 95%	[77]
MnO ₂ /g-C ₃ N ₄ (MG3)	MO	visible light	50 mg	100 mL 5 mg/L	100 min 92%	[251]
Fe ₃ O ₄ /C/MnO ₂ /C ₃ N ₄	MO	400 W metal halide lamp	20 mg	20 mL 10 mg/L	140 min 94.11%	[249]

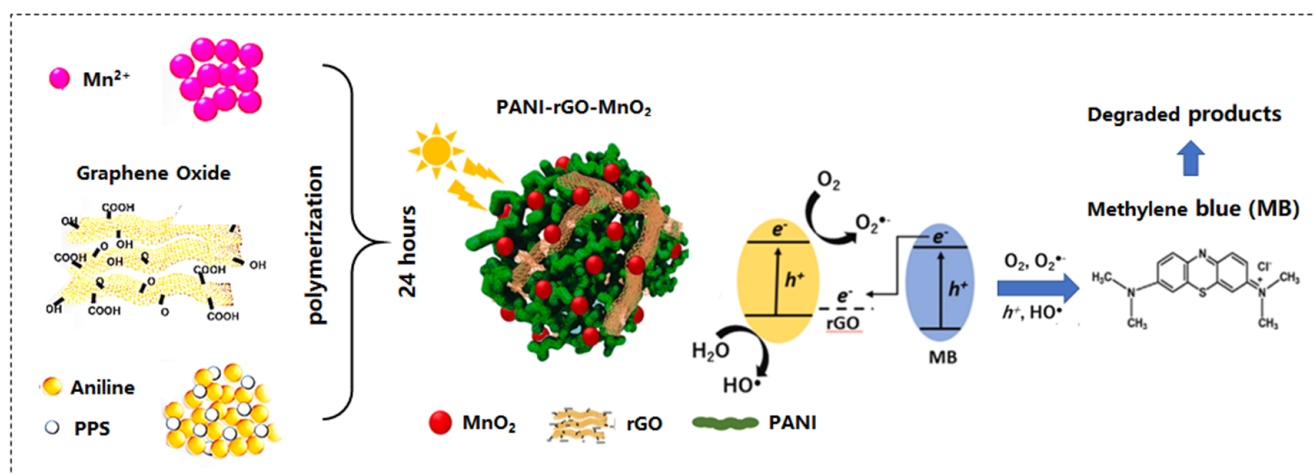


Figure 4. Application schematic illustration of the ternary PANI-rGO-MnO₂ composite for photocatalytic degradation of organic dye MB under sunlight irradiation. Figures reprinted with permission from ref. [250]. Copyright 2021; Elsevier Ltd.

3.4. Heavy Metal Wastewater

The high solubility, bioaccumulation, and non-biodegradability of heavy metals make them easily accumulate in living beings through the food chain and drinking water [252–254]. The heavy metals entering the organism are easy to bind with essential cellular components such as proteins, nucleic acids, and enzymes, destroying organic cells in the body and endangering the health of organisms and human bodies [195,255]. However, the toxicity, mutagenicity, and carcinogenicity of heavy metals are strongly dependent on the oxidation state [256]. Reducing a high-valence state and highly toxic heavy metal ion into a low-valence state and low-toxic or non-toxic heavy metal ion is an effective way to mitigate the potential hazards of heavy metals [257–259].

It has been reported that MnO₂-carbon materials can be used as photocatalysts to reduce toxic heavy metals to non-toxic metals using light energy. Padhi et al. [260] reported a highly efficient hydrothermal method to fabricate an RGO/ α -MnO₂ nanorod composite, which showed outstanding photoreduction ability. A 97% reduction in Cr(VI) under visible light irradiation for 2 h and no significant loss of photoreduction ability up to the third cycle. Wang et al. [261] prepared MnO₂@g-C₃N₄ composite photocatalyst by compounding MnO₂ on g-C₃N₄ via the hydrothermal method for the treatment of uranium-containing wastewater. Under optimal conditions, the photocatalytic reduction rate of U(VI) reached 96.3% under visible light irradiation for 120 min. There is little research on the photoreduction of heavy metals by MnO₂-carbon materials, and related applications still need further exploration.

4. Conclusions and Outlook

Photocatalytic technology has attracted extensive attention from researchers because of its green, energy-saving, and high efficiency. It is significant to develop low-cost and non-toxic, environmentally friendly photocatalysts. MnO₂ and carbon materials are commonly green and low-cost materials, the composite methods are simple and diverse, and different methods can synthesize photocatalytic materials of various dimensions and sizes. Compared with a single photocatalyst, the photocatalytic activity of MnO₂-carbon composites is significantly improved, and a variety of pollutants can be removed efficiently. At present, many synthetic methods have been developed to prepare MnO₂-carbon materials for degrading various pollutants, but the practical application is still in the early stage, and no major breakthrough has been made. The transition from the laboratory to the actual water body is still facing great challenges. In future research, the following aspects need further exploration and development.

(1) The performance optimization of MnO₂-carbon materials. The photocatalytic efficiency of MnO₂-carbon composites is mostly around 80% or 90%, and the photocatalytic activity needs to be improved further. Therefore, the improvement of photocatalytic performance of MnO₂-carbon materials is the core problem of photocatalytic technology improvement, and the proportion and preparation process of MnO₂-carbon composite material fundamentally determine its photocatalytic performance. On the one hand, the properties of MnO₂-carbon materials can be optimized by adjusting the ratio of MnO₂ and carbon materials. On the other hand, it can be improved by doping metal or nonmetal, adding polymers, oxides, or other carbon materials.

(2) The separation and recovery of MnO₂-carbon materials. Powdered MnO₂-carbon materials not only have the disadvantages that cannot be dispersed evenly and recovered difficulty, but the quantitative loss during the recycling process may influence the fate of adsorbed contaminants, thus causing potential environmental risks. Therefore, it is necessary to explore effective methods to prepare high-dimensional materials that are more conducive to recycling, such as hydrogels, aerogels, and flexible films. Compared with low-dimensional materials, high-dimensional materials have broader prospects in practical applications.

(3) The large-scale application of photocatalytic technology. The application of photocatalytic treatment of MnO₂-carbon materials mostly stays in the laboratory stage, and it is

difficult to use it on a large scale. To achieve large-scale utilization, we need to consider the cost, stability, and quantifiable productivity of photocatalysts. Therefore, it is necessary to explore 3D MnO₂-carbon materials with better stability, enlarge the size of materials in equal proportion and test their properties, improve the reuse rate of the materials, and reduce the material costs. The stability of MnO₂-carbon materials and the amplified photocatalytic performance are crucial issues to be solved to realize the large-scale application of photocatalytic technology.

(4) The research on MnO₂-carbon materials in actual water treatment. Most of the MnO₂-carbon materials are studied for single pollutants, but the pollutants in actual water bodies have complex components, various kinds, and different concentrations, which are far more complicated than the laboratory simulation. Therefore, we need to evaluate the ability of MnO₂-carbon materials as a photocatalyst to treat multiple pollutants simultaneously, explore the potential adverse effects of multiple pollutants, develop different sizes and types of MnO₂-carbon materials, select the study area, collect wastewater samples from actual water bodies, and study the photocatalytic performance of MnO₂-carbon materials for actual wastewater treatment. The use of MnO₂-carbon materials for photocatalytic degradation of various organic pollutants in water bodies, from laboratory study to practical water application, is a major challenge and a key research direction for the future.

Author Contributions: Conceptualization, Q.C.; investigation, K.F. and Y.L.; data curation, K.F.; writing—original draft preparation, K.F. and Q.C.; writing—review and editing, Q.C.; supervision, Q.C.; project administration, Q.C.; funding acquisition, Q.C. and J.Z. All authors have read and agreed to the published version of the manuscript.

Funding: Supported by Budget Surplus of Central Financial Science and Technology Plan: 2021-JY-04.

Data Availability Statement: Where no new data were created.

Conflicts of Interest: The authors declare no conflict of interest.

References

1. Santhosh, C.; Velmurugan, V.; Jacob, G.; Jeong, S.K.; Grace, A.N.; Bhatnagar, A. Role of nanomaterials in water treatment applications: A review. *Chem. Eng. J.* **2016**, *306*, 1116–1137. [[CrossRef](#)]
2. Zhang, X.; Wang, J.; Dong, X.-X.; Lv, Y.-K. Functionalized metal-organic frameworks for photocatalytic degradation of organic pollutants in environment. *Chemosphere* **2020**, *242*, 125144. [[CrossRef](#)]
3. Fang, H.; Zhang, H.; Han, L.; Mei, J.; Ge, Q.; Long, Z.; Yu, Y. Exploring bacterial communities and biodegradation genes in activated sludge from pesticide wastewater treatment plants via metagenomic analysis. *Environ. Pollut.* **2018**, *243*, 1206–1216. [[CrossRef](#)] [[PubMed](#)]
4. Khan, A.; Wang, J.; Li, J.; Wang, X.; Chen, Z.; Alsaedi, A.; Hayat, T.; Chen, Y.; Wang, X. The role of graphene oxide and graphene oxide-based nanomaterials in the removal of pharmaceuticals from aqueous media: A review. *Environ. Sci. Pollut. Res.* **2017**, *24*, 7938–7958. [[CrossRef](#)] [[PubMed](#)]
5. Nidheesh, P.V.; Zhou, M.; Oturan, M.A. An overview on the removal of synthetic dyes from water by electrochemical advanced oxidation processes. *Chemosphere* **2018**, *197*, 210–227. [[CrossRef](#)]
6. Wu, Y.; Pang, H.; Liu, Y.; Wang, X.; Yu, S.; Fu, D.; Chen, J.; Wang, X. Environmental remediation of heavy metal ions by novel-nanomaterials: A review. *Environ. Pollut.* **2019**, *246*, 608–620. [[CrossRef](#)] [[PubMed](#)]
7. Wen, T.; Wang, J.; Yu, S.; Chen, Z.; Hayat, T.; Wang, X. Magnetic Porous Carbonaceous Material Produced from Tea Waste for Efficient Removal of As(V), Cr(VI), Humic Acid, and Dyes. *ACS Sustain. Chem. Eng.* **2017**, *5*, 4371–4380. [[CrossRef](#)]
8. Liu, X.; Ma, R.; Wang, X.; Ma, Y.; Yang, Y.; Zhuang, L.; Zhang, S.; Jehan, R.; Chen, J.; Wang, X. Graphene oxide-based materials for efficient removal of heavy metal ions from aqueous solution: A review. *Environ. Pollut.* **2019**, *252*, 62–73. [[CrossRef](#)]
9. Guo, N.; Zeng, Y.; Li, H.; Xu, X.; Yu, H.; Han, X. Novel mesoporous TiO₂@g-C₃N₄ hollow core@shell heterojunction with enhanced photocatalytic activity for water treatment and H₂ production under simulated sunlight. *J. Hazard. Mater.* **2018**, *353*, 80–88. [[CrossRef](#)]
10. Li, R.; Li, T.; Zhou, Q. Impact of Titanium Dioxide (TiO₂) Modification on Its Application to Pollution Treatment—A Review. *Catalysts* **2020**, *10*, 804. [[CrossRef](#)]
11. Saha, D.; Hoinkis, T.J.; Van Bramer, S.E. Electrospun, flexible and reusable nanofiber mat of graphitic carbon nitride: Photocatalytic reduction of hexavalent chromium. *J. Colloid Interface Sci.* **2020**, *575*, 433–442. [[CrossRef](#)] [[PubMed](#)]
12. Chiu, K.-L.; Lin, L.-Y. Applied potential-dependent performance of the nickel cobalt oxysulfide nanotube/nickel molybdenum oxide nanosheet core-shell structure in energy storage and oxygen evolution. *J. Mater. Chem. A* **2019**, *7*, 4626–4639. [[CrossRef](#)]

13. Zhu, Y.; Chen, G.; Chu, Y.-C.; Hsu, C.-S.; Wang, J.; Tung, C.-W.; Chen, H.M. Hetero-Atomic Pairs with a Distal Fe³⁺-Site Boost Water Oxidation. *Angew. Chem.-Int. Ed.* **2022**, *61*, e202211142. [[CrossRef](#)] [[PubMed](#)]
14. Okoro, G.; Husain, S.; Saukani, M.; Mutalik, C.; Yougbare, S.; Hsiao, Y.-C.; Kuo, T.-R. Emerging Trends in Nanomaterials for Photosynthetic Biohybrid Systems. *ACS Mater. Lett.* **2022**, *5*, 95–115. [[CrossRef](#)]
15. Das, S.; Sarnanta, A.; Jana, S. Light-Assisted Synthesis of Hierarchical Flower-Like MnO₂ Nanocomposites with Solar Light Induced Enhanced Photocatalytic Activity. *ACS Sustain. Chem. Eng.* **2017**, *5*, 9086–9094. [[CrossRef](#)]
16. Sienkiewicz, A.; Wanag, A.; Kusiak-Nejman, E.; Ekiert, E.; Rokicka-Konieczna, P.; Morawski, A.W. Effect of calcination on the photocatalytic activity and stability of TiO₂ photocatalysts modified with APTES. *J. Environ. Chem. Eng.* **2021**, *9*, 104794. [[CrossRef](#)]
17. Zhang, G.; Chen, D.; Li, N.; Xu, Q.; Li, H.; He, J.; Lu, J. Fabrication of Bi₂MoO₆/ZnO hierarchical heterostructures with enhanced visible-light photocatalytic activity. *Appl. Catal. B-Environ.* **2019**, *250*, 313–324. [[CrossRef](#)]
18. Babar, S.; Gayade, N.; Shinde, H.; Mahajan, P.; Lee, K.H.; Mane, N.; Deshmukh, A.; Garadkar, K.; Bhuse, V. Evolution of Waste Iron Rust into Magnetically Separable g-C₃N₄-Fe₂O₃ Photocatalyst: An Efficient and Economical Waste Management Approach. *ACS Appl. Nano Mater.* **2018**, *1*, 4682–4694. [[CrossRef](#)]
19. Li, D.; Huang, J.; Li, R.; Chen, P.; Chen, D.; Cai, M.; Liu, H.; Feng, Y.; Lv, W.; Liu, G. Synthesis of a carbon dots modified g-C₃N₄/SnO₂ Z-scheme photocatalyst with superior photocatalytic activity for PPCPs degradation under visible light irradiation. *J. Hazard. Mater.* **2021**, *401*, 123257. [[CrossRef](#)]
20. Kudo, A.; Miseki, Y. Heterogeneous photocatalyst materials for water splitting. *Chem. Soc. Rev.* **2009**, *38*, 253–278. [[CrossRef](#)]
21. Sharma, S.; Dutta, V.; Singh, P.; Raizada, P.; Rahmani-Sani, A.; Hosseini-Bandegharai, A.; Thakur, V.K. Carbon quantum dot supported semiconductor photocatalysts for efficient degradation of organic pollutants in water: A review. *J. Clean. Prod.* **2019**, *228*, 755–769. [[CrossRef](#)]
22. Han, T.; Xie, C.M.; Meng, Y.J.; Wei, Y. Synthesized MnO₂/Ag/g-C₃N₄ composite for photoreduction carbon dioxide under visible light. *J. Mater. Sci.-Mater. Electron.* **2018**, *29*, 20984–20990. [[CrossRef](#)]
23. Zhang, S.; Li, B.; Wang, X.; Zhao, G.; Hu, B.; Lu, Z.; Wen, T.; Chen, J.; Wang, X. Recent developments of two-dimensional graphene-based composites in visible-light photocatalysis for eliminating persistent organic pollutants from wastewater. *Chem. Eng. J.* **2020**, *390*, 124642. [[CrossRef](#)]
24. Sakai, N.; Ebina, Y.; Takada, K.; Sasaki, T. Photocurrent generation from semiconducting manganese oxide nanosheets in response to visible light. *J. Phys. Chem. B* **2005**, *109*, 9651–9655. [[CrossRef](#)] [[PubMed](#)]
25. Zhao, H.; Zhang, G.; Zhang, Q. MnO₂/CeO₂ for catalytic ultrasonic degradation of methyl orange. *Ultrason. Sonochem.* **2014**, *21*, 991–996. [[CrossRef](#)] [[PubMed](#)]
26. Zhang, L.; Lian, J.; Wu, L.; Duan, Z.; Jiang, J.; Zhao, L. Synthesis of a Thin-Layer MnO₂ Nanosheet-Coated Fe₃O₄ Nanocomposite as a Magnetically Separable Photocatalyst. *Langmuir* **2014**, *30*, 7006–7013. [[CrossRef](#)]
27. Wu, Z.; Chen, X.; Yuan, B.; Fu, M.-L. A facile foaming-polymerization strategy to prepare 3D MnO₂ modified biochar-based porous hydrogels for efficient removal of Cd(II) and Pb(II). *Chemosphere* **2020**, *239*, 124745. [[CrossRef](#)]
28. Cao, H.; Suib, S.L. Highly efficient heterogeneous photooxidation of 2-propanol to acetone with amorphous manganese oxide catalysts. *J. Am. Chem. Soc.* **1994**, *116*, 5334–5342. [[CrossRef](#)]
29. Hang, Y.; Zhang, C.; Luo, X.; Xie, Y.; Xin, S.; Li, Y.; Zhang, D.; Goodenough, J.B. alpha-MnO₂ nanorods supported on porous graphitic carbon nitride as efficient electrocatalysts for lithium-air batteries. *J. Power Sources* **2018**, *392*, 15–22. [[CrossRef](#)]
30. Salari, H. Efficient photocatalytic degradation of environmental pollutant with enhanced photocarrier separation in novel Z-scheme a-MnO₂/nanorod/a-MoO₃ nanocomposites. *J. Photochem. Photobiol. A-Chem.* **2020**, *401*, 112787. [[CrossRef](#)]
31. Singh, M.; Thanh, D.N.; Ulbrich, P.; Strnadova, N.; Stepanek, F. Synthesis, characterization and study of arsenate adsorption from aqueous solution by alpha- and delta-phase manganese dioxide nanoadsorbents. *J. Solid State Chem.* **2010**, *183*, 2979–2986. [[CrossRef](#)]
32. Samanta, A.; Pal, S.K.; Jana, S. Exploring flowery MnO₂/Ag nanocomposite as an efficient solar-light-driven photocatalyst. *New J. Chem.* **2022**, *46*, 4189–4197. [[CrossRef](#)]
33. Yang, W.; Su, Z.a.; Xu, Z.; Yang, W.; Peng, Y.; Li, J. Comparative study of alpha-, beta-, gamma- and delta-MnO₂ on toluene oxidation: Oxygen vacancies and reaction intermediates. *Appl. Catal. B-Environ.* **2020**, *260*, 118150. [[CrossRef](#)]
34. Baral, A.; Satish, L.; Zhang, G.; Ju, S.; Ghosh, M.K. A Review of Recent Progress on Nano MnO₂: Synthesis, Surface Modification and Applications. *J. Inorg. Organomet. Polym. Mater.* **2021**, *31*, 899–922. [[CrossRef](#)]
35. Chiam, S.-L.; Pung, S.-Y.; Yeoh, F.-Y. Recent developments in MnO₂-based photocatalysts for organic dye removal: A review. *Environ. Sci. Pollut. Res.* **2020**, *27*, 5759–5778. [[CrossRef](#)] [[PubMed](#)]
36. Genuino, H.C.; Dharmarathna, S.; Njagi, E.C.; Mei, M.C.; Suib, S.L. Gas-Phase Total Oxidation of Benzene, Toluene, Ethylbenzene, and Xylenes Using Shape-Selective Manganese Oxide and Copper Manganese Oxide Catalysts. *J. Phys. Chem. C* **2012**, *116*, 12066–12078. [[CrossRef](#)]
37. Saputra, E.; Muhammad, S.; Sun, H.; Ang, H.M.; Tade, M.O.; Wang, S. Different Crystallographic One-dimensional MnO₂ Nanomaterials and Their Superior Performance in Catalytic Phenol Degradation. *Environ. Sci. Technol.* **2013**, *47*, 5882–5887. [[CrossRef](#)]
38. Ma, L.; Li, D.; Wang, L.; Ma, X. In situ hydrothermal synthesis of alpha-MnO₂ nanowire/activated carbon hollow fibers from cotton stalk composite: Dual-effect cyclic visible light photocatalysis performance. *Cellulose* **2020**, *27*, 8937–8948. [[CrossRef](#)]

39. Baral, A.; Das, D.P.; Minakshi, M.; Ghosh, M.K.; Padhi, D.K. Probing Environmental Remediation of RhB Organic Dye Using alpha-MnO₂ under Visible- Light Irradiation: Structural, Photocatalytic and Mineralization Studies. *Chemistryselect* **2016**, *1*, 4277–4285. [[CrossRef](#)]
40. Mishra, B.P.; Acharya, L.; Subudhi, S.; Parida, K. Oxygen vacancy rich a-MnO₂ @B/O-g-C₃N₄ photocatalyst: A thriving 1D-2D surface interaction effective towards photocatalytic O(2) and H-2 evolution through Z-scheme charge dynamics. *Int. J. Hydrog. Energy* **2022**, *47*, 32107–32120. [[CrossRef](#)]
41. Sekar, S.; Lee, S.; Vijayarangan, P.; Kalirajan, K.M.; Santhakumar, T.; Sekar, S.; Sadhasivam, S. Upcycling of Wastewater via Effective Photocatalytic Hydrogen Production Using MnO₂ Nanoparticles-Decorated Activated Carbon Nanoflakes. *Nanomaterials* **2020**, *10*, 1610. [[CrossRef](#)] [[PubMed](#)]
42. Xu, H.; Jia, J.; Guo, Y.; Qu, Z.; Liao, Y.; Xie, J.; Shangguan, W.; Yan, N. Design of 3D MnO₂/Carbon sphere composite for the catalytic oxidation and adsorption of elemental mercury. *J. Hazard. Mater.* **2018**, *342*, 69–76. [[CrossRef](#)] [[PubMed](#)]
43. Chhabra, T.; Kumar, A.; Bahuguna, A.; Krishnan, V. Reduced graphene oxide supported MnO₂ nanorods as recyclable and efficient adsorptive photocatalysts for pollutants removal. *Vacuum* **2019**, *160*, 333–346. [[CrossRef](#)]
44. Ong, W.-J.; Putri, L.K.; Mohamed, A.R. Rational Design of Carbon-Based 2D Nanostructures for Enhanced Photocatalytic CO(2)Reduction: A Dimensionality Perspective. *Chem.-A Eur. J.* **2020**, *26*, 9710–9748. [[CrossRef](#)] [[PubMed](#)]
45. Tian, M.-J.; Liao, F.; Ke, Q.-F.; Guo, Y.-J.; Guo, Y.-P. Synergetic effect of titanium dioxide ultralong nanofibers and activated carbon fibers on adsorption and photodegradation of toluene. *Chem. Eng. J.* **2017**, *328*, 962–976. [[CrossRef](#)]
46. Teng, F.; Zhang, G.; Wang, Y.; Gao, C.; Chen, L.; Zhang, P.; Zhang, Z.; Xie, E. The role of carbon in the photocatalytic reaction of carbon/TiO₂ photocatalysts. *Appl. Surf. Sci.* **2014**, *320*, 703–709. [[CrossRef](#)]
47. Cui, G.-W.; Wang, W.-L.; Ma, M.-Y.; Zhang, M.; Xia, X.-Y.; Han, F.-Y.; Shi, X.-F.; Zhao, Y.-Q.; Dong, Y.-B.; Tang, B. Rational design of carbon and TiO₂ assembly materials: Covered or strewn, which is better for photocatalysis? *Chem. Commun.* **2013**, *49*, 6415–6417. [[CrossRef](#)]
48. Theerthagiri, J.; Chandrasekaran, S.; Salla, S.; Elakkiya, V.; Senthil, R.A.; Nithyadharseni, P.; Maiyalagan, T.; Micheal, K.; Ayeshamariam, A.; Arasu, M.V.; et al. Recent developments of metal oxide based heterostructures for photocatalytic applications towards environmental remediation. *J. Solid State Chem.* **2018**, *267*, 35–52. [[CrossRef](#)]
49. Park, S.K.; Suh, D.H.; Park, H.S. Electrochemical assembly of reduced graphene oxide/manganese dioxide nanocomposites into hierarchical sea urchin-like structures for supercapacitive electrodes. *J. Alloys Compd.* **2016**, *668*, 146–151. [[CrossRef](#)]
50. Guan, S.; Li, W.; Ma, J.; Lei, Y.; Zhu, Y.; Huang, Q.; Dou, X. A review of the preparation and applications of MnO₂ composites in formaldehyde oxidation. *J. Ind. Eng. Chem.* **2018**, *66*, 126–140. [[CrossRef](#)]
51. Qiu, B.; Xing, M.; Zhang, J. Recent advances in three-dimensional graphene based materials for catalysis applications. *Chem. Soc. Rev.* **2018**, *47*, 2165–2216. [[CrossRef](#)]
52. Huang, D.; Li, Z.; Zeng, G.; Zhou, C.; Xue, W.; Gong, X.; Yan, X.; Chen, S.; Wang, W.; Cheng, M. Megamerger in photocatalytic field: 2D g-C₃N₄ nanosheets serve as support of 0D nanomaterials for improving photocatalytic performance. *Appl. Catal. B-Environ.* **2019**, *240*, 153–173. [[CrossRef](#)]
53. Chen, J.; Qiu, F.; Xu, W.; Cao, S.; Zhu, H. Recent progress in enhancing photocatalytic efficiency of TiO₂-based materials. *Appl. Catal. A-Gen.* **2015**, *495*, 131–140. [[CrossRef](#)]
54. Fernando, K.A.S.; Sahu, S.; Liu, Y.; Lewis, W.K.; Gulians, E.A.; Jafariyan, A.; Wang, P.; Bunker, C.E.; Sun, Y.-P. Carbon Quantum Dots and Applications in Photocatalytic Energy Conversion. *ACS Appl. Mater. Interfaces* **2015**, *7*, 8363–8376. [[CrossRef](#)]
55. Hung, M.-C.; Yuan, S.-Y.; Hung, C.-C.; Cheng, C.-L.; Ho, H.-C.; Ko, T.-H. Effectiveness of ZnO/carbon-based material as a catalyst for photodegradation of acrolein. *Carbon* **2014**, *66*, 93–104. [[CrossRef](#)]
56. Zou, W.; Gao, B.; Ok, Y.S.; Dong, L. Integrated adsorption and photocatalytic degradation of volatile organic compounds (VOCs) using carbon-based nanocomposites: A critical review. *Chemosphere* **2019**, *218*, 845–859. [[CrossRef](#)] [[PubMed](#)]
57. Georgakilas, V.; Perman, J.A.; Tucek, J.; Zboril, R. Broad Family of Carbon Nanoallotropes: Classification, Chemistry, and Applications of Fullerenes, Carbon Dots, Nanotubes, Graphene, Nanodiamonds, and Combined Superstructures. *Chem. Rev.* **2015**, *115*, 4744–4822. [[CrossRef](#)]
58. Tang, K.; Hong, T.Z.X.; You, L.; Zhou, K. Carbon-metal compound composite electrodes for capacitive deionization: Synthesis, development and applications. *J. Mater. Chem. A* **2019**, *7*, 26693–26743. [[CrossRef](#)]
59. Zhu, S.; Huo, W.; Liu, X.; Zhang, Y. Birnessite based nanostructures for supercapacitors: Challenges, strategies and prospects. *Nanoscale Adv.* **2020**, *2*, 37–54. [[CrossRef](#)]
60. Yu, J.; Wang, G.; Cheng, B.; Zhou, M. Effects of hydrothermal temperature and time on the photocatalytic activity and microstructures of bimodal mesoporous TiO₂ powders. *Appl. Catal. B-Environ.* **2007**, *69*, 171–180. [[CrossRef](#)]
61. Pang, H.; Wu, Y.; Wang, X.; Hu, B.; Wang, X. Recent Advances in Composites of Graphene and Layered Double Hydroxides for Water Remediation: A Review. *Chem.-Asian J.* **2019**, *14*, 2542–2552. [[CrossRef](#)] [[PubMed](#)]
62. Xiang, Q.; Yu, J.; Jaroniec, M. Graphene-based semiconductor photocatalysts. *Chem. Soc. Rev.* **2012**, *41*, 782–796. [[CrossRef](#)] [[PubMed](#)]
63. Chang, H.; Wu, H. Graphene-based nanocomposites: Preparation, functionalization, and energy and environmental applications. *Energy Environ. Sci.* **2013**, *6*, 3483–3507. [[CrossRef](#)]
64. Li, Q.; Li, X.; Wageh, S.; Al-Ghamdi, A.A.; Yu, J. CdS/Graphene Nanocomposite Photocatalysts. *Adv. Energy Mater.* **2015**, *5*, 1500010. [[CrossRef](#)]

65. Song, Z.; Ma, Y.-L.; Li, C.-E. The residual tetracycline in pharmaceutical wastewater was effectively removed by using MnO₂/graphene nanocomposite. *Sci. Total Environ.* **2019**, *651*, 580–590. [[CrossRef](#)] [[PubMed](#)]
66. Mo, Z.; Xu, H.; Chen, Z.; She, X.; Song, Y.; Lian, J.; Zhu, X.; Yan, P.; Lei, Y.; Yuan, S.; et al. Construction of MnO₂/Monolayer g-C₃N₄ with Mn vacancies for Z-scheme overall water splitting. *Appl. Catal. B-Environ.* **2019**, *241*, 452–460. [[CrossRef](#)]
67. Shi, Y.; Zhang, M.; Li, Y.; Liu, G.; Jin, R.; Wang, Q.; Xu, H.; Gao, S. 2D/1D protonated g-C₃N₄/alpha-MnO₂ Z-scheme heterojunction with enhanced visible-light photocatalytic efficiency. *Ceram. Int.* **2020**, *46*, 25905–25914. [[CrossRef](#)]
68. Chen, T.; Jiang, S.; Li, L.; Qian, K.; Sun, J.; Guo, W.; Cai, X.; Yu, K. Vertically aligned MnO₂ nanostructures on carbon fibers with tunable electromagnetic wave absorption performance. *Appl. Surf. Sci.* **2022**, *589*, 152858. [[CrossRef](#)]
69. Lv, H.; Gao, X.; Xu, Q.; Liu, H.; Wang, Y.-G.; Xia, Y. Carbon Quantum Dot-Induced MnO₂ Nanowire Formation and Construction of a Binder-Free Flexible Membrane with Excellent Superhydrophilicity and Enhanced Supercapacitor Performance. *ACS Appl. Mater. Interfaces* **2017**, *9*, 40394–40403. [[CrossRef](#)]
70. Wu, M.; Kwok, Y.H.; Zhang, Y.; Szeto, W.; Huang, H.; Leung, D.Y.C. Synergetic effect of vacuum ultraviolet photolysis and ozone catalytic oxidation for toluene degradation over MnO₂-rGO composite catalyst. *Chem. Eng. Sci.* **2021**, *231*, 116288c. [[CrossRef](#)]
71. Hao, L.; Li, S.-S.; Wang, J.; Tan, Y.; Bai, L.; Liu, A. MnO₂/multi-walled carbon nanotubes based nanocomposite with enhanced electrocatalytic activity for sensitive amperometric glucose biosensing. *J. Electroanal. Chem.* **2020**, *878*, 114602. [[CrossRef](#)]
72. Yu, L.; Mo, Z.; Zhu, X.; Deng, J.; Xu, F.; Song, Y.; She, Y.; Li, H.; Xu, H. Construction of 2D/2D Z-scheme MnO₂-x/g-C₃N₄ photocatalyst for efficient nitrogen fixation to ammonia. *Green Energy Environ.* **2021**, *6*, 538–545. [[CrossRef](#)]
73. Shi, J.; Wang, S.; Wang, Q.; Chen, X.; Du, X.; Wang, M.; Zhao, Y.; Dong, C.; Ruan, L.; Zeng, W. A new flexible zinc-ion capacitor based on delta-MnO₂@Carbon cloth battery-type cathode and MXene@Cotton cloth capacitor-type anode. *J. Power Sources* **2020**, *446*, 227345. [[CrossRef](#)]
74. Xu, Z.; Sun, S.; Cui, W.; Lv, J.; Geng, Y.; Li, H.; Deng, J. Interconnected network of ultrafine MnO₂ nanowires on carbon cloth with weed-like morphology for high-performance supercapacitor electrodes. *Electrochim. Acta* **2018**, *268*, 340–346. [[CrossRef](#)]
75. Wang, Z.; Yu, H.; Zhang, L.; Guo, L.; Dong, X. Photothermal conversion of graphene/layered manganese oxide 2D/2D composites for room-temperature catalytic purification of gaseous formaldehyde. *J. Taiwan Inst. Chem. Eng.* **2020**, *107*, 119–128. [[CrossRef](#)]
76. Wang, Q.; Ma, Y.; Liang, X.; Zhang, D.; Miao, M. Flexible supercapacitors based on carbon nanotube-MnO₂ nanocomposite film electrode. *Chem. Eng. J.* **2019**, *371*, 145–153. [[CrossRef](#)]
77. Singh, R.; Kumar, M.; Tashi, L.; Khajuria, H.; Sheikh, H.N. Hydrothermal synthesis of manganese oxide and nitrogen doped graphene (NG-MnO₂) nanohybrid for visible light degradation of methyl orange dye. *Mol. Phys.* **2019**, *117*, 2477–2486. [[CrossRef](#)]
78. Liu, W.-X.; Zhu, X.-L.; Li, S.-Q.; Gu, Q.-Q.; Meng, Z.-D. Near-Infrared-Driven Selective Photocatalytic Removal of Ammonia Based on Valence Band Recognition of an alpha-MnO₂/N-Doped Graphene Hybrid Catalyst. *ACS Omega* **2018**, *3*, 5537–5546. [[CrossRef](#)]
79. Dong, J.; Lu, G.; Wu, F.; Xu, C.; Kang, X.; Cheng, Z. Facile synthesis of a nitrogen-doped graphene flower-like MnO₂ nanocomposite and its application in supercapacitors. *Appl. Surf. Sci.* **2018**, *427*, 986–993. [[CrossRef](#)]
80. Poochai, C.; Sriprachubwong, C.; Sodditpinta, J.; Lohitkarn, J.; Pasakon, P.; Primpray, V.; Maeboonruan, N.; Lomas, T.; Wisitsoraat, A.; Tuantranont, A. Alpha-MnO₂ nanofibers/nitrogen and sulfur-co-doped reduced graphene oxide for 4.5 V quasi-solid state supercapacitors using ionic liquid-based polymer electrolyte. *J. Colloid Interface Sci.* **2021**, *583*, 734–745. [[CrossRef](#)]
81. Zhu, J.; Xu, Y.; Hu, J.; Wei, L.; Liu, J.; Zheng, M. Facile synthesis of MnO₂ grown on nitrogen-doped carbon nanotubes for asymmetric supercapacitors with enhanced electrochemical performance. *J. Power Sources* **2018**, *393*, 135–144. [[CrossRef](#)]
82. Dewangan, L.; Korram, J.; Karbhal, I.; Nagwanshi, R.; Satnami, M.L. N-Doped Carbon Quantum Dot-MnO₂ Nanowire FRET Pairs: Detection of Cholesterol, Glutathione, Acetylcholinesterase, and Chlorpyrifos. *ACS Appl. Nano Mater.* **2021**, *4*, 13612–13624. [[CrossRef](#)]
83. Bano, D.; Chandra, S.; Yadav, P.K.; Singh, V.K.; Hasan, S.H. Off-on detection of glutathione based on the nitrogen, sulfur codoped carbon quantum dots@MnO₂ nano-composite in human lung cancer cells and blood serum. *J. Photochem. Photobiol. A-Chem.* **2020**, *398*, 112558. [[CrossRef](#)]
84. Li, J.; Luo, S.; Liu, G.; Wan, J.; Lu, J.; Li, B.; Han, X.; Hu, C. A high-performance asymmetric supercapacitor achieved by surface-regulated MnO₂ and organic-framework-derived N-doped carbon cloth. *Mater. Today Chem.* **2021**, *22*, 100620. [[CrossRef](#)]
85. Zhong, R.; Xu, M.; Fu, N.; Liu, R.; Zhou, A.A.; Wang, X.; Yang, Z. A flexible high-performance symmetric quasi-solid supercapacitor based on Ni-doped MnO₂ nano-array @ carbon cloth. *Electrochim. Acta* **2020**, *348*, 136209. [[CrossRef](#)]
86. Wang, J.; Zhou, H.; Wang, Z.; Bai, W.; Cao, Y.; Wei, Y. Constructing hierarchical structure based on LDH anchored boron-doped g-C₃N₄ assembled with MnO₂ nanosheets towards reducing toxicants generation and fire hazard of epoxy resin. *Compos. Part B-Eng.* **2022**, *229*, 109453. [[CrossRef](#)]
87. Shan, Q.Y.; Guo, X.L.; Dong, F.; Zhang, Y.X. Single atom (K/Na) doped graphitic carbon Nitride@ MnO₂ as an efficient electrode Material for supercapacitor. *Mater. Lett.* **2017**, *202*, 103–106. [[CrossRef](#)]
88. Wan, H.; Ge, H.; Zhang, L.; Duan, T. CS@MnO₂ core-shell nanospheres with enhanced visible light photocatalytic degradation. *Mater. Lett.* **2019**, *237*, 290–293. [[CrossRef](#)]
89. Wang, N.; Wu, L.; Li, J.; Mo, J.; Peng, Q.; Li, X. Construction of hierarchical Fe₂O₃@MnO₂ core/shell nanocube supported C₃N₄ for dual Z-scheme photocatalytic water splitting. *Sol. Energy Mater. Sol. Cells* **2020**, *215*, 110624. [[CrossRef](#)]
90. Asif, M.; Rashad, M.; Ali, Z.; Qiu, H.; Li, W.; Pan, L.; Hou, Y. Ni-doped MnO₂/CNT nanoarchitectures as a cathode material for ultra-long life magnesium/lithium hybrid ion batteries. *Mater. Today Energy* **2018**, *10*, 108–117. [[CrossRef](#)]

91. Qu, J.; Shi, L.; He, C.; Gao, F.; Li, B.; Zhou, Q.; Hu, H.; Shao, G.; Wang, X.; Qiu, J. Highly efficient synthesis of graphene/MnO₂ hybrids and their application for ultrafast oxidative decomposition of methylene blue. *Carbon* **2014**, *66*, 485–492. [[CrossRef](#)]
92. Lv, H.; Yuan, Y.; Xu, Q.; Liu, H.; Wang, Y.-G.; Xia, Y. Carbon quantum dots anchoring MnO₂/graphene aerogel exhibits excellent performance as electrode materials for supercapacitor. *J. Power Sources* **2018**, *398*, 167–174. [[CrossRef](#)]
93. Tuan Sang, T.; Tripathi, K.M.; Kim, B.N.; You, I.-K.; Park, B.J.; Han, Y.H.; Kim, T. Three-dimensionally assembled Graphene/alpha-MnO₂ nanowire hybrid hydrogels for high performance supercapacitors. *Mater. Res. Bull.* **2017**, *96*, 395–404. [[CrossRef](#)]
94. Ren, Y.; Xu, Q.; Zhang, J.; Yang, H.; Wang, B.; Yang, D.; Hu, J.; Liu, Z. Functionalization of Biomass Carbonaceous Aerogels: Selective Preparation of MnO₂@CA Composites for Supercapacitors. *ACS Appl. Mater. Interfaces* **2014**, *6*, 9689–9697. [[CrossRef](#)] [[PubMed](#)]
95. Jia, L.; Shi, Y.; Zhang, Q.; Xu, X. Green synthesis of ultrafine Methyl-cellulose-derived porous carbon/MnO₂ nanowires for asymmetric supercapacitors and flexible pattern stamping. *Appl. Surf. Sci.* **2018**, *462*, 923–931. [[CrossRef](#)]
96. Zhang, N.; Fu, C.; Liu, D.; Li, Y.; Zhou, H.; Kuang, Y. Three-Dimensional Pompon-like MnO₂/Graphene Hydrogel Composite for Supercapacitor. *Electrochim. Acta* **2016**, *210*, 804–811. [[CrossRef](#)]
97. Teimuri-Mofrad, R.; Payami, E.; Piriniya, A.; Hadi, R. Green synthesis of ferrocenyl-modified MnO₂/carbon-based nanocomposite as an outstanding supercapacitor electrode material. *Appl. Organomet. Chem.* **2022**, *36*, e6620. [[CrossRef](#)]
98. Niu, Z.; Yue, T.; Hu, W.; Sun, W.; Hu, Y.; Xu, Z. Covalent bonding of MnO₂ onto graphene aerogel forwards: Efficiently catalytic degradation of organic wastewater. *Appl. Surf. Sci.* **2019**, *496*, 143585. [[CrossRef](#)]
99. Dong, Q.; Wang, J.; Duan, X.; Tan, X.; Liu, S.; Wang, S. Self-assembly of 3D MnO₂/N-doped graphene hybrid aerogel for catalytic degradation of water pollutants: Structure-dependent activity. *Chem. Eng. J.* **2019**, *369*, 1049–1058. [[CrossRef](#)]
100. Wang, Z.; Han, Y.; Fan, W.; Wang, Y.; Huang, L. Shell-core MnO₂/Carbon@Carbon nanotubes synthesized by a facile one-pot method for peroxydisulfate oxidation of tetracycline. *Sep. Purif. Technol.* **2022**, *278*, 119558. [[CrossRef](#)]
101. Zhou, H.; Lu, Y.; Wu, F.; Fang, L.; Luo, H.; Zhang, Y.; Zhou, M. MnO₂ nanorods/MXene/CC composite electrode for flexible supercapacitors with enhanced electrochemical performance. *J. Alloys Compd.* **2019**, *802*, 259–268. [[CrossRef](#)]
102. Ghosh, K.; Yue, C.Y.; Sk, M.M.; Jena, R.K.; Bi, S. Development of a 3D graphene aerogel and 3D porous graphene/MnO₂@polyaniline hybrid film for all-solid-state flexible asymmetric supercapacitors. *Sustain. Energy Fuels* **2018**, *2*, 280–293. [[CrossRef](#)]
103. Iqbal, J.; Ansari, M.O.; Numan, A.; Wageh, S.; Al-Ghamdi, A.; Alam, M.G.; Kumar, P.; Jafer, R.; Bashir, S.; Rajpar, A.H. Hydrothermally Assisted Synthesis of Porous Polyaniline@Carbon Nanotubes-Manganese Dioxide Ternary Composite for Potential Application in Supercapattery. *Polymers* **2020**, *12*, 2918. [[CrossRef](#)] [[PubMed](#)]
104. Xu, Z.; Sun, S.; Cui, W.; Yu, D.; Deng, J. Ultrafine MnO₂ nanowires grown on RGO-coated carbon cloth as a binder-free and flexible supercapacitor electrode with high performance. *RSC Adv.* **2018**, *8*, 38631–38640. [[CrossRef](#)] [[PubMed](#)]
105. Li, S.; Zhao, Y.; Liu, Z.; Yang, L.; Zhang, J.; Wang, M.; Che, R. Flexible Graphene-Wrapped Carbon Nanotube/Graphene@MnO₂ 3D Multilevel Porous Film for High-Performance Lithium-Ion Batteries. *Small* **2018**, *14*, e1801007. [[CrossRef](#)]
106. Tong, L.; Qiu, F.; Zeng, T.; Long, J.; Yang, J.; Wang, R.; Zhang, J.; Wang, C.; Sun, T.; Yang, Y. Recent progress in the preparation and application of quantum dots/graphene composite materials. *RSC Adv.* **2017**, *7*, 47999–48018. [[CrossRef](#)]
107. Xu, N.; Liu, J.; Qiao, J.; Huang, H.; Zhou, X.-D. Interweaving between MnO₂ nanowires/nanorods and carbon nanotubes as robust multifunctional electrode for both liquid and flexible electrochemical energy devices. *J. Power Sources* **2020**, *455*, 227992. [[CrossRef](#)]
108. Zhang, X.; Liu, Y.; Chen, L.; Li, Z.; Qu, Y.; Wu, W.; Jing, L. Porous two-dimension MnO₂-C₃N₄/titanium phosphate nanocomposites as efficient photocatalysts for CO oxidation and mechanisms. *Appl. Catal. B-Environ.* **2021**, *282*, 119563. [[CrossRef](#)]
109. Chao, G.; Zhang, L.; Yuan, S.; Xue, T.; Yang, F.; Huang, Y.; Fan, W.; Liu, T. Ultrathin MnO₂ Sheet Arrays Grown on Hollow Carbon Fibers as Effective Polysulfide-Blocking Interlayers for High-Performance Li-S Batteries. *ACS Appl. Energy Mater.* **2020**, *3*, 12703–12708. [[CrossRef](#)]
110. Sivaraj, D.; Vijayalakshmi, K. Preferential killing of bacterial cells by hybrid carbon nanotube-MnO₂ nanocomposite synthesized by novel microwave assisted processing. *Mater. Sci. Eng. C-Mater. Biol. Appl.* **2017**, *81*, 469–477. [[CrossRef](#)]
111. Li, M.; Chen, Q.; Zhan, H. Ultrathin manganese dioxide nanosheets grown on partially unzipped nitrogen-doped carbon nanotubes for high-performance asymmetric supercapacitors. *J. Alloys Compd.* **2017**, *702*, 236–243. [[CrossRef](#)]
112. Sridhar, V.; Lee, I.; Jung, K.H.; Park, H. Metal Organic Framework Derived MnO₂-Carbon Nanotubes for Efficient Oxygen Reduction Reaction and Arsenic Removal from Contaminated Water. *Nanomaterials* **2020**, *10*, 1895. [[CrossRef](#)] [[PubMed](#)]
113. Xu, Y.; Shi, G.; Duan, X. Self-Assembled Three-Dimensional Graphene Macrostructures: Synthesis and Applications in Supercapacitors. *Acc. Chem. Res.* **2015**, *48*, 1666–1675. [[CrossRef](#)]
114. Khamsanga, S.; Nguyen, M.T.; Yonezawa, T.; Thamyongkit, P.; Pornprasertsuk, R.; Pattananuwat, P.; Tuantranont, A.; Siwamogsatham, S.; Kheawhom, S. MnO(2)Heterostructure on Carbon Nanotubes as Cathode Material for Aqueous Zinc-Ion Batteries. *Int. J. Mol. Sci.* **2020**, *21*, 4689. [[CrossRef](#)]
115. Guo, J.; Chen, T.; Zhou, X.; Zheng, T.; Xia, W.; Zhong, C.; Liu, Y. Preparation and Pb (II) adsorption in aqueous of 2D/2D g-C₃N₄/MnO₂ composite. *Appl. Organomet. Chem.* **2019**, *33*, e5119. [[CrossRef](#)]
116. Xu, J.; Li, D.; Chen, Y.; Tan, L.; Kou, B.; Wan, F.; Jiang, W.; Li, F. Constructing Sheet-On-Sheet Structured Graphitic Carbon Nitride/Reduced Graphene Oxide/Layered MnO₂ Ternary Nanocomposite with Outstanding Catalytic Properties on Thermal Decomposition of Ammonium Perchlorate. *Nanomaterials* **2017**, *7*, 450. [[CrossRef](#)] [[PubMed](#)]
117. Han, Q.; Zhang, W.; Han, Z.; Wang, F.; Geng, D.; Li, X.; Li, Y.; Zhang, X. Preparation of PAN-based carbon fiber@MnO₂ composite as an anode material for structural lithium-ion batteries. *J. Mater. Sci.* **2019**, *54*, 11972–11982. [[CrossRef](#)]

118. Ji, T.; Zhang, S.; He, Y.; Zhang, X.; Zhang, X.; Li, W. Enhanced thermoelectric property of cement-based materials with the synthesized MnO₂/carbon fiber composite. *J. Build. Eng.* **2021**, *43*, 103190. [[CrossRef](#)]
119. Corpuz, R.D.; De Juan, L.M.Z.; Praserttham, S.; Pomprasertsuk, R.; Yonezawa, T.; Mai Thanh, N.; Kheawhom, S. Annealing induced a well-ordered single crystal delta-MnO₂ and its electrochemical performance in zinc-ion battery. *Sci. Rep.* **2019**, *9*, 15107. [[CrossRef](#)]
120. Ou, X.; Li, Q.; Xu, D.; Guo, J.; Yan, F. In Situ Growth of MnO₂ Nanosheets on N-Doped Carbon Nanotubes Derived from Polypyrrole Tubes for Supercapacitors. *Chem. Asian J.* **2018**, *13*, 545–551. [[CrossRef](#)]
121. Wang, D.; Wang, K.; Sun, L.; Wu, H.; Wang, J.; Zhao, Y.; Yan, L.; Luo, Y.; Jiang, K.; Li, Q.; et al. MnO₂ nanoparticles anchored on carbon nanotubes with hybrid supercapacitor-battery behavior for ultrafast lithium storage. *Carbon* **2018**, *139*, 145–155. [[CrossRef](#)]
122. Wei, J.; Liu, Y.; Ding, Y.; Luo, C.; Du, X.; Lin, J. MnO₂ spontaneously coated on carbon nanotubes for enhanced water oxidation. *Chem. Commun.* **2014**, *50*, 11938–11941. [[CrossRef](#)]
123. Zhang, L.; Tian, Y.; Song, C.; Qiu, H.; Xue, H. Study on preparation and performance of flexible all-solid-state supercapacitor based on nitrogen-doped RGO/CNT/MnO₂ composite fibers. *J. Alloys Compd.* **2021**, *859*, 157816. [[CrossRef](#)]
124. Liu, Q.; Hu, Z.; Li, L.; Li, W.; Zou, C.; Jin, H.; Wang, S.; Chou, S.-L. Facile Synthesis of Birnessite delta-MnO₂ and Carbon Nanotube Composites as Effective Catalysts for Li-CO₂ Batteries. *ACS Appl. Mater. Interfaces* **2021**, *13*, 16585–16593. [[CrossRef](#)] [[PubMed](#)]
125. Wu, B.; Li, Y.; Su, K.; Tan, L.; Liu, X.; Cui, Z.; Yang, X.; Liang, Y.; Li, Z.; Zhu, S.; et al. The enhanced photocatalytic properties of MnO₂/g-C₃N₄ heterostructure for rapid sterilization under visible light. *J. Hazard. Mater.* **2019**, *377*, 227–236. [[CrossRef](#)] [[PubMed](#)]
126. Singu, B.S.; Goda, E.S.; Yoon, K.R. Carbon Nanotube-Manganese oxide nanorods hybrid composites for high-performance supercapacitor materials. *J. Ind. Eng. Chem.* **2021**, *97*, 239–249. [[CrossRef](#)]
127. Wang, M.; Shen, M.; Zhang, L.; Tian, J.; Jin, X.; Zhou, Y.; Shi, J. 2D-2D MnO₂/g-C₃N₄ heterojunction photocatalyst: In-situ synthesis and enhanced CO₂ reduction activity. *Carbon* **2017**, *120*, 23–31. [[CrossRef](#)]
128. Peng, S.; Yang, X.; Strong, J.; Sarkar, B.; Jiang, Q.; Peng, F.; Liu, D.; Wang, H. MnO₂-decorated N-doped carbon nanotube with boosted activity for low-temperature oxidation of formaldehyde. *J. Hazard. Mater.* **2020**, *396*, 122750. [[CrossRef](#)] [[PubMed](#)]
129. Wang, J.; Chen, B.; Xing, B. Wrinkles and Folds of Activated Graphene Nanosheets as Fast and Efficient Adsorptive Sites for Hydrophobic Organic Contaminants. *Environ. Sci. Technol.* **2016**, *50*, 3798–3808. [[CrossRef](#)]
130. Wang, J.; Chen, B. Adsorption and coadsorption of organic pollutants and a heavy metal by graphene oxide and reduced graphene materials. *Chem. Eng. J.* **2015**, *281*, 379–388. [[CrossRef](#)]
131. Zhao, J.; Wang, Z.; White, J.C.; Xing, B. Graphene in the Aquatic Environment: Adsorption, Dispersion, Toxicity and Transformation. *Environ. Sci. Technol.* **2014**, *48*, 9995–10009. [[CrossRef](#)]
132. Dong, Y.-D.; Zhang, H.; Zhong, G.-J.; Yao, G.; Lai, B. Cellulose/carbon Composites and their Applications in Water Treatment—A Review. *Chem. Eng. J.* **2021**, *405*, 126980. [[CrossRef](#)]
133. Liang, J.; Xu, Y.; Huang, Y.; Zhang, L.; Wang, Y.; Ma, Y.; Li, F.; Guo, T.; Chen, Y. Infrared-Triggered Actuators from Graphene-Based Nanocomposites. *J. Phys. Chem. C* **2009**, *113*, 9921–9927. [[CrossRef](#)]
134. Sun, H.; Xu, Z.; Gao, C. Multifunctional, Ultra-Flyweight, Synergistically Assembled Carbon Aerogels. *Adv. Mater.* **2013**, *25*, 2554–2560. [[CrossRef](#)] [[PubMed](#)]
135. Liu, J.; Ge, X.; Ye, X.; Wang, G.; Zhang, H.; Zhou, H.; Zhang, Y.; Zhao, H. 3D graphene/delta-MnO₂ aerogels for highly efficient and reversible removal of heavy metal ions. *J. Mater. Chem. A* **2016**, *4*, 1970–1979. [[CrossRef](#)]
136. Zhou, J.; Pei, Z.; Li, N.; Han, S.; Li, Y.; Chen, Q.; Sui, Z. Synthesis of 3D graphene/MnO₂ nanocomposites with hierarchically porous structure for water purification. *J. Porous Mater.* **2022**, *29*, 983–990. [[CrossRef](#)]
137. Lai, F.; Huang, Y.; Zuo, L.; Gu, H.; Miao, Y.-E.; Liu, T. Electrospun nanofiber-supported carbon aerogel as a versatile platform toward asymmetric supercapacitors. *J. Mater. Chem. A* **2016**, *4*, 15861–15869. [[CrossRef](#)]
138. Jyothibasu, J.P.; Wang, R.-H.; Ong, K.; Ong, J.H.L.; Lee, R.-H. Cellulose/carbon nanotube/MnO₂ composite electrodes with high mass loadings for symmetric supercapacitors. *Cellulose* **2021**, *28*, 3549–3567. [[CrossRef](#)]
139. Tang, C.; Zhao, K.; Tang, Y.; Li, F.; Meng, Q. Forest-like carbon foam templated rGO/CNTs/MnO₂ electrode for high-performance supercapacitor. *Electrochim. Acta* **2021**, *375*, 137960. [[CrossRef](#)]
140. He, S.; Xiao, K.; Chen, X.-Z.; Li, T.; Ouyang, T.; Wang, Z.; Guo, M.-L.; Liu, Z.-Q. Enhanced photoelectrocatalytic activity of direct Z-scheme porous amorphous carbon nitride/manganese dioxide nanorod arrays. *J. Colloid Interface Sci.* **2019**, *557*, 644–654. [[CrossRef](#)]
141. Zhang, J.; Sun, J.; Shifa, T.A.; Wang, D.; Wu, X.; Cui, Y. Hierarchical MnO₂/activated carbon cloth electrode prepared by synchronized electrochemical activation and oxidation for flexible asymmetric supercapacitors. *Chem. Eng. J.* **2019**, *372*, 1047–1055. [[CrossRef](#)]
142. Kataoka, F.; Ishida, T.; Nagita, K.; Kumbhar, V.; Yamabuki, K.; Nakayama, M. Cobalt-Doped Layered MnO₂ Thin Film Electrochemically Grown on Nitrogen-Doped Carbon Cloth for Aqueous Zinc-Ion Batteries. *ACS Appl. Energy Mater.* **2020**, *3*, 4720–4726. [[CrossRef](#)]
143. Ko, W.-Y.; Liu, Y.-C.; Lai, J.-Y.; Chung, C.-C.; Lin, K.-J. Vertically Standing MnO₂ Nanowalls Grown on AgCNT-Modified Carbon Fibers for High-Performance Supercapacitors. *ACS Sustain. Chem. Eng.* **2019**, *7*, 669. [[CrossRef](#)]
144. Chen, M.; Cheng, Q.; Qian, Y.; He, J.; Dong, X. Alkali cation incorporated MnO₂ cathode and carbon cloth anode for flexible aqueous supercapacitor with high wide-voltage and power density. *Electrochim. Acta* **2020**, *342*, 136046. [[CrossRef](#)]

145. Lin, Y.-H.; Wei, T.-Y.; Chien, H.-C.; Lu, S.-Y. Manganese Oxide/Carbon Aerogel Composite: An Outstanding Supercapacitor Electrode Material. *Adv. Energy Mater.* **2011**, *1*, 901–907. [[CrossRef](#)]
146. He, Y.; Chen, W.; Li, X.; Zhang, Z.; Fu, J.; Zhao, C.; Xie, E. Freestanding Three-Dimensional Graphene/MnO₂ Composite Networks As Ultra light and Flexible Supercapacitor Electrodes. *ACS Nano* **2013**, *7*, 174–182. [[CrossRef](#)]
147. Zhu, Y.; Xu, H.; Chen, P.; Bao, Y.; Jiang, X.; Chen, Y. Electrochemical performance of polyaniline-coated gamma-MnO₂ on carbon cloth as flexible electrode for supercapacitor. *Electrochim. Acta* **2022**, *413*, 140146. [[CrossRef](#)]
148. Li, G.-R.; Feng, Z.-P.; Ou, Y.-N.; Wu, D.; Fu, R.; Tong, Y.-X. Mesoporous MnO₂/Carbon Aerogel Composites as Promising Electrode Materials for High-Performance Supercapacitors. *Langmuir* **2010**, *26*, 2209–2213. [[CrossRef](#)]
149. Liu, Y.; Chi, X.; Han, Q.; Du, Y.; Huang, J.; Liu, Y.; Yang, J. alpha-MnO₂ nanofibers/carbon nanotubes hierarchically assembled microspheres: Approaching practical applications of high-performance aqueous Zn-ion batteries. *J. Power Sources* **2019**, *443*, 227244. [[CrossRef](#)]
150. Wang, Y.; Zhang, D.; Lu, Y.; Wang, W.; Peng, T.; Zhang, Y.; Guo, Y.; Wang, Y.; Huo, K.; Kim, J.-K.; et al. Cable-like double-carbon layers for fast ion and electron transport: An example of CNT@NCT@MnO₂ 3D nanostructure for high-performance supercapacitors. *Carbon* **2019**, *143*, 335–342. [[CrossRef](#)]
151. Xu, J.; Hou, K.; Ju, Z.; Ma, C.; Wang, W.; Wang, C.; Cao, J.; Chen, Z. Synthesis and Electrochemical Properties of Carbon Dots/Manganese Dioxide (CQDs/MnO₂) Nanoflowers for Supercapacitor Applications. *J. Electrochem. Soc.* **2017**, *164*, A430–A437. [[CrossRef](#)]
152. Saharan, P.; Sharma, A.K.; Kumar, V.; Kaushal, I. Multifunctional CNT supported metal doped MnO₂ composite for adsorptive removal of anionic dye and thiourea sensing. *Mater. Chem. Phys.* **2019**, *221*, 239–249. [[CrossRef](#)]
153. Wadi, V.S.; Ibrahim, Y.; Arangadi, A.F.; Kilybay, A.; Mavukkandy, M.O.; Alhseinat, E.; Hasan, S.W. Three-dimensional graphene/MWCNT-MnO₂ nanocomposites for high-performance capacitive deionization (CDI) application. *J. Electroanal. Chem.* **2022**, *914*, 116318. [[CrossRef](#)]
154. Hong, S.; Huang, X.; Liu, H.; Gao, Z. In Situ Chemical Synthesis of MnO₂/HMCNT Nanocomposite with a Uniquely Developed Three-Dimensional Open Porous Architecture for Supercapacitors. *J. Inorg. Organomet. Polym. Mater.* **2019**, *29*, 1587–1596. [[CrossRef](#)]
155. Zeng, X.; Shan, C.; Sun, M.; Ding, D.; Rong, S. Graphene enhanced α -MnO₂ for photothermal catalytic decomposition of carcinogen formaldehyde. *Chin. Chem. Lett.* **2022**, *33*, 4771–4775.
156. Kumar, V.; Saharan, P.; Sharma, A.K.; Umar, A.; Kaushal, I.; Mittal, A.; Al-Hadeethi, Y.; Rashad, B. Silver doped manganese oxide-carbon nanotube nanocomposite for enhanced dye-sequestration: Isotherm studies and RSM modelling approach. *Ceram. Int.* **2020**, *46*, 10309–10319. [[CrossRef](#)]
157. Xia, P.; Zhu, B.; Cheng, B.; Yu, J.; Xu, J. 2D/2D g-C₃N₄/MnO₂ Nanocomposite as a Direct Z-Scheme Photocatalyst for Enhanced Photocatalytic Activity. *ACS Sustain. Chem. Eng.* **2018**, *6*, 965–973. [[CrossRef](#)]
158. Wu, F.; Gao, X.; Xu, X.; Jiang, Y.; Gao, X.; Yin, R.; Shi, W.; Liu, W.; Lu, G.; Cao, X. MnO₂ Nanosheet-Assembled Hollow Polyhedron Grown on Carbon Cloth for Flexible Aqueous Zinc-Ion Batteries. *ChemSuschem* **2020**, *13*, 1537–1545. [[CrossRef](#)]
159. Lee, K.G.; Jeong, J.-M.; Lee, S.J.; Yeom, B.; Lee, M.-K.; Choi, B.G. Sonochemical-assisted synthesis of 3D graphene/nanoparticle foams and their application in supercapacitor. *Ultrason. Sonochem.* **2015**, *22*, 422–428. [[CrossRef](#)]
160. Le, Q.J.; Huang, M.; Wang, T.; Liu, X.Y.; Sun, L.; Guo, X.L.; Jiang, D.B.; Wang, J.; Dong, F.; Zhang, Y.X. Biotemplate derived three dimensional nitrogen doped graphene@MnO₂ as bifunctional material for supercapacitor and oxygen reduction reaction catalyst. *J. Colloid Interface Sci.* **2019**, *544*, 155–163. [[CrossRef](#)] [[PubMed](#)]
161. Shan, Q.Y.; Guan, B.; Zhu, S.J.; Zhang, H.J.; Zhang, Y.X. Facile synthesis of carbon-doped graphitic C₃N₄@MnO₂ with enhanced electrochemical performance. *RSC Adv.* **2016**, *6*, 83209–83216. [[CrossRef](#)]
162. Kaur, M.; Kaur, M.; Sharma, V.K. Nitrogen-doped graphene and graphene quantum dots: A review on synthesis and applications in energy, sensors and environment. *Adv. Colloid Interface Sci.* **2018**, *259*, 44–64. [[CrossRef](#)] [[PubMed](#)]
163. Li, Q.; Xia, Y.; Wan, X.; Yang, S.; Cai, Z.; Ye, Y.; Li, G. Morphology-dependent MnO₂/nitrogen-doped graphene nanocomposites for simultaneous detection of trace dopamine and uric acid. *Mater. Sci. Eng. C-Mater. Biol. Appl.* **2020**, *109*, 110615. [[CrossRef](#)] [[PubMed](#)]
164. Choudhury, B.J.; Moholkar, V.S. Ultrasound-assisted facile one-pot synthesis of ternary MWCNT/MnO₂/rGO nanocomposite for high performance supercapacitors with commercial-level mass loadings. *Ultrason. Sonochem.* **2022**, *82*, 105896. [[CrossRef](#)] [[PubMed](#)]
165. Majumdar, D.; Bhattacharya, S.K. Sonochemically synthesized hydroxy-functionalized graphene-MnO₂ nanocomposite for supercapacitor applications. *J. Appl. Electrochem.* **2017**, *47*, 789–801. [[CrossRef](#)]
166. Naderi, H.R.; Norouzi, P.; Ganjali, M.R. Electrochemical study of a novel high performance supercapacitor based on MnO₂/nitrogen-doped graphene nanocomposite. *Appl. Surf. Sci.* **2016**, *366*, 552–560. [[CrossRef](#)]
167. Majumdar, D.; Bhattacharya, S.K. Synthesis, Characterization and Electrochemical Study of Hydroxy-Functionalized Graphene/MnO₂ Nanocomposite. In Proceedings of the International Conference on Materials Research and Applications (ICMRA), Hyderabad, India, 11–13 March 2016; pp. 3872–3877.
168. Wang, M.; Yan, Q.; Xue, F.; Zhang, J.; Wang, J. Design and synthesis of carbon nanotubes/carbon fiber/reduced graphene oxide/MnO₂ flexible electrode material for supercapacitors. *J. Phys. Chem. Solids* **2018**, *119*, 29–35. [[CrossRef](#)]

169. Yashas, S.R.; Shivaraju, H.P.; Pema, G.; Swamy, N.K.; Namratha, K.; Gurupadaya, B.; Madhusudan, P. Sonochemical synthesis of graphitic carbon nitride-manganese oxide interfaces for enhanced photocatalytic degradation of tetracycline hydrochloride. *Environ. Sci. Pollut. Res.* **2021**, *28*, 4778–4789. [[CrossRef](#)]
170. Chai, C.; Yang, X.; Yang, X.; Dong, C.; Bian, W.; Choi, M.M.F. An ultrasensitive MnO₂-S,O-doped g-C₃N₄ nanoprobe for "turn-on" detection of glutathione and cell imaging. *J. Mater. Sci.* **2022**, *57*, 7909–7922. [[CrossRef](#)]
171. Zhang, Y.; Li, H.; Zhang, L.; Gao, R.; Dai, W.-L. Construction of Highly Efficient 3D/2D MnO₂/g-C₃N₄ Nanocomposite in the Epoxidation of Styrene with TBHP. *ACS Sustain. Chem. Eng.* **2019**, *7*, 17008–17019. [[CrossRef](#)]
172. Zhang, Q.; Peng, Y.; Deng, F.; Wang, M.; Chen, D. Porous Z-scheme MnO₂/Mn-modified alkalized g-C₃N₄ heterojunction with excellent Fenton-like photocatalytic activity for efficient degradation of pharmaceutical pollutants. *Sep. Purif. Technol.* **2020**, *246*, 116890. [[CrossRef](#)]
173. Anbumannan, V.; Dinesh, M.; Kumar, R.T.R.; Suresh, K. Hierarchical alpha-MnO₂ wrapped MWCNTs sensor for low level detection of p-nitrophenol in water. *Ceram. Int.* **2019**, *45*, 23097–23103. [[CrossRef](#)]
174. Jia, H.; Cai, Y.; Zheng, X.; Lin, J.; Liang, H.; Qi, J.; Cao, J.; Feng, J.; Fei, W. Mesostructured Carbon Nanotube-on-MnO₂ Nanosheet Composite for High-Performance Supercapacitors. *ACS Appl. Mater. Interfaces* **2018**, *10*, 38963–38969. [[CrossRef](#)] [[PubMed](#)]
175. Abdullah, N.; Othman, F.E.C.; Yusof, N.; Matsuura, T.; Lau, W.J.; Jaafar, J.; Ismail, A.F.; Salleh, W.N.W.; Aziz, F. Preparation of nanocomposite activated carbon nanofiber/manganese oxide and its adsorptive performance toward leads (II) from aqueous solution. *J. Water Process Eng.* **2020**, *37*, 101430. [[CrossRef](#)]
176. Wei, B.; Wang, L.; Wang, Y.; Yuan, Y.; Miao, Q.; Yang, Z.; Fei, W. In situ growth of manganese oxide on 3D graphene by a reverse microemulsion method for supercapacitors. *J. Power Sources* **2016**, *307*, 129–137. [[CrossRef](#)]
177. Zhu, X.; Zhang, P.; Xu, S.; Yan, X.; Xue, Q. Free-Standing Three-Dimensional Graphene/Manganese Oxide Hybrids As Binder-Free Electrode Materials for Energy Storage Applications. *ACS Appl. Mater. Interfaces* **2014**, *6*, 11665–11674. [[CrossRef](#)]
178. Pang, H.; Abdalla, A.M.; Sahu, R.P.; Duan, Y.; Puri, I.K. Low-temperature synthesis of manganese oxide-carbon nanotube-enhanced microwave-absorbing nanocomposites. *J. Mater. Sci.* **2018**, *53*, 16288–16302. [[CrossRef](#)]
179. Wang, Z.; Yu, H.; Xiao, Y.; Zhang, L.; Guo, L.; Zhang, L.; Dong, X. Free-standing composite films of multiple 2D nanosheets: Synergetic photothermocatalysis/photocatalysis for efficient removal of formaldehyde under ambient condition. *Chem. Eng. J.* **2020**, *394*, 125014. [[CrossRef](#)]
180. Hasija, V.; Nguyen, V.-H.; Kumar, A.; Raizada, P.; Krishnan, V.; Khan, A.A.P.; Singh, P.; Lichtfouse, E.; Wang, C.; Huong, P.T. Advanced activation of persulfate by polymeric g-C₃N₄ based photocatalysts for environmental remediation: A review. *J. Hazard. Mater.* **2021**, *413*, 125324. [[CrossRef](#)]
181. Sonu; Dutta, V.; Sharma, S.; Raizada, P.; Hosseini-Bandegharai, A.; Gupta, V.K.; Singh, P. Review on augmentation in photocatalytic activity of CoFe₂O₄ via heterojunction formation for photocatalysis of organic pollutants in water. *J. Saudi Chem. Soc.* **2019**, *23*, 1119–1136. [[CrossRef](#)]
182. Zuo, W.; Zhang, L.; Zhang, Z.; Tang, S.; Sun, Y.; Huang, H.; Yu, Y. Degradation of organic pollutants by intimately coupling photocatalytic materials with microbes: A review. *Crit. Rev. Biotechnol.* **2021**, *41*, 273–299. [[CrossRef](#)] [[PubMed](#)]
183. Gomez-Pastora, J.; Dominguez, S.; Bringas, E.; Rivero, M.J.; Ortiz, I.; Dionysiou, D.D. Review and perspectives on the use of magnetic nanophotocatalysts (MNPCs) in water treatment. *Chem. Eng. J.* **2017**, *310*, 407–427. [[CrossRef](#)]
184. Pal, A.; He, Y.; Jekel, M.; Reinhard, M.; Gin, K.Y.-H. Emerging contaminants of public health significance as water quality indicator compounds in the urban water cycle. *Environ. Int.* **2014**, *71*, 46–62. [[CrossRef](#)]
185. Syafrudin, M.; Kristanti, R.A.; Yuniarto, A.; Hadibarata, T.; Rhee, J.; Al-onazi, W.A.; Algarni, T.S.; Almarri, A.H.; Al-Mohaimed, A.M. Pesticides in Drinking Water-A Review. *Int. J. Environ. Res. Public Health* **2021**, *18*, 468. [[CrossRef](#)]
186. Tho Chau Minh Vinh, D.; Duy Quoc, N.; Kien Trung, N.; Phuoc Huu, L. TiO₂ and Au-TiO₂ Nanomaterials for Rapid Photocatalytic Degradation of Antibiotic Residues in Aquaculture Wastewater. *Materials* **2019**, *12*, 2434. [[CrossRef](#)]
187. Jalloul, G.; Keniar, I.; Tehrani, A.; Boyadjian, C. Antibiotics Contaminated Irrigation Water: An Overview on Its Impact on Edible Crops and Visible Light Active Titania as Potential Photocatalysts for Irrigation Water Treatment. *Front. Environ. Sci.* **2021**, *9*, 767963. [[CrossRef](#)]
188. Pandiyan, R.; Dharmaraj, S.; Ayyaru, S.; Sugumaran, A.; Somasundaram, J.; Kazi, A.S.; Samiappan, S.C.; Ashokkumar, V.; Ngamcharussrivichai, C. Ameliorative photocatalytic dye degradation of hydrothermally synthesized bimetallic Ag-Sn hybrid nanocomposite treated upon domestic wastewater under visible light irradiation. *J. Hazard. Mater.* **2022**, *421*, 126734. [[CrossRef](#)] [[PubMed](#)]
189. Qian, C.; Yin, J.; Zhao, J.; Li, X.; Wang, S.; Bai, Z.; Jiao, T. Facile preparation and highly efficient photodegradation performances of self-assembled Artemia eggshell-ZnO nanocomposites for wastewater treatment. *Colloids Surf. A-Physicochem. Eng. Asp.* **2021**, *610*, 125752. [[CrossRef](#)]
190. Hasija, V.; Raizada, P.; Sudhaik, A.; Sharma, K.; Kumar, A.; Singh, P.; Jonnalagadda, S.B.; Thakur, V.K. Recent advances in noble metal free doped graphitic carbon nitride based nanohybrids for photocatalysis of organic contaminants in water: A review. *Appl. Mater. Today* **2019**, *15*, 494–524. [[CrossRef](#)]
191. Yang, F.; Du, M.; Yin, K.; Qiu, Z.; Zhao, J.; Liu, C.; Zhang, G.; Gao, Y.; Pang, H. Applications of Metal-Organic Frameworks in Water Treatment: A Review. *Small* **2022**, *18*, 2105715. [[CrossRef](#)]
192. Koe, W.S.; Lee, J.W.; Chong, W.C.; Pang, Y.L.; Sim, L.C. An overview of photocatalytic degradation: Photocatalysts, mechanisms, and development of photocatalytic membrane. *Environ. Sci. Pollut. Res.* **2020**, *27*, 2522–2565. [[CrossRef](#)] [[PubMed](#)]

193. Kumar, A.; Aathira, M.S.; Pal, U.; Jain, S.L. Photochemical Oxidative Coupling of 2-Naphthols using a Hybrid Reduced Graphene Oxide/Manganese Dioxide Nanocomposite under Visible-Light Irradiation. *Chemcatchem* **2018**, *10*, 1844–1852. [[CrossRef](#)]
194. Teh, C.M.; Mohamed, A.R. Roles of titanium dioxide and ion-doped titanium dioxide on photocatalytic degradation of organic pollutants (phenolic compounds and dyes) in aqueous solutions: A review. *J. Alloys Compd.* **2011**, *509*, 1648–1660. [[CrossRef](#)]
195. Ren, G.; Han, H.; Wang, Y.; Liu, S.; Zhao, J.; Meng, X.; Li, Z. Recent Advances of Photocatalytic Application in Water Treatment: A Review. *Nanomaterials* **2021**, *11*, 1804. [[CrossRef](#)]
196. Biglari, H.; Afsharnia, M.; Alipour, V.; Khosravi, R.; Sharafi, K.; Mahvi, A.H. A review and investigation of the effect of nanophotocatalytic ozonation process for phenolic compound removal from real effluent of pulp and paper industry. *Environ. Sci. Pollut. Res.* **2017**, *24*, 4105–4116. [[CrossRef](#)]
197. Said, K.A.M.; Ismail, A.F.; Karim, Z.A.; Abdullah, M.S.; Hafeez, A. A review of technologies for the phenolic compounds recovery and phenol removal from wastewater. *Process Saf. Environ. Prot.* **2021**, *151*, 257–289. [[CrossRef](#)]
198. Ramos-Ramirez, E.; Tzompantzi-Morales, F.; Gutierrez-Ortega, N.; Mojica-Calvillo, H.G.; Castillo-Rodriguez, J. Photocatalytic Degradation of 2,4,6-Trichlorophenol by MgO-MgFe₂O₄ Derived from Layered Double Hydroxide Structures. *Catalysts* **2019**, *9*, 454. [[CrossRef](#)]
199. Shobha, P.; Paul Winston, A.J.P.; Sunil, S.; David, T.M.; Margaret, S.M.; Muthupandi, S.; Sagayaraj, P. Facile Synthesis of rGO/Mn₃O₄ Composite for Efficient Photodegradation of Phenol under Visible Light. *J. Nanomater.* **2021**, *2021*, 5576048. [[CrossRef](#)]
200. Jabbar, Z.H.; Graimed, B.H. Recent developments in industrial organic degradation via semiconductor heterojunctions and the parameters affecting the photocatalytic process: A review study. *J. Water Process Eng.* **2022**, *47*, 102671. [[CrossRef](#)]
201. Al-Mamun, M.R.; Kader, S.; Islam, M.S.; Khan, M.Z.H. Photocatalytic activity improvement and application of UV-TiO₂ photocatalysis in textile wastewater treatment: A review. *J. Environ. Chem. Eng.* **2019**, *7*, 103248. [[CrossRef](#)]
202. Zhou, M.; Zhang, J.; Sun, C. Occurrence, Ecological and Human Health Risks, and Seasonal Variations of Phenolic Compounds in Surface Water and Sediment of a Potential Polluted River Basin in China. *Int. J. Environ. Res. Public Health* **2017**, *14*, 1140. [[CrossRef](#)] [[PubMed](#)]
203. Motamedi, M.; Yerushalmi, L.; Haghghat, F.; Chen, Z. Recent developments in photocatalysis of industrial effluents: A review and example of phenolic compounds degradation. *Chemosphere* **2022**, *296*, 133688. [[CrossRef](#)]
204. Malakootian, M.; Heidari, M.R. Removal of phenol from steel wastewater by combined electrocoagulation with photo-Fenton. *Water Sci. Technol.* **2018**, *78*, 1260–1267. [[CrossRef](#)] [[PubMed](#)]
205. Li, X.; Huang, G.; Chen, X.; Huang, J.; Li, M.; Yin, J.; Liang, Y.; Yao, Y.; Li, Y. A review on graphitic carbon nitride (g-C₃N₄) based hybrid membranes for water and wastewater treatment. *Sci. Total Environ.* **2021**, *792*, 148462. [[CrossRef](#)] [[PubMed](#)]
206. Eryilmaz, C.; Genc, A. Review of Treatment Technologies for the Removal of Phenol from Wastewaters. *J. Water Chem. Technol.* **2021**, *43*, 145–154. [[CrossRef](#)]
207. Mehta, A.; Mishra, A.; Basu, S. Fluorescent carbon dot decorated MnO₂ nanorods for complete photomineralization of phenol from water. *Environ. Sci.-Water Res. Technol.* **2018**, *4*, 2012–2020. [[CrossRef](#)]
208. Salam, M.A.; Mohamed, R.M.; Obaid, A.Y. Enhancement of Titanium Dioxide-Manganese Oxide Nanoparticles Photocatalytic Activity by Doping with Multi-walled Carbon Nanotubes. *Fuller. Nanotub. Carbon Nanostruct.* **2014**, *22*, 765–779. [[CrossRef](#)]
209. Xavier, S.S.J.; Siva, G.; Ranjani, M.; Rani, S.D.; Priyanga, N.; Srinivasan, R.; Pannipara, M.; Al-Sehemi, A.G.; Kumar, G.G. Turn-on fluorescence sensing of hydrazine using MnO₂ nanotube-decorated g-C₃N₄ nanosheets. *New J. Chem.* **2019**, *43*, 13196–13204. [[CrossRef](#)]
210. Pan, X.; Kong, F.; Xing, M. Spatial separation of photo-generated carriers in g-C₃N₄/MnO₂/Pt with enhanced H₂ evolution and organic pollutant control. *Res. Chem. Intermed.* **2022**, *48*, 2837–2855. [[CrossRef](#)]
211. Yasmeen, H.; Zada, A.; Liu, S. Dye loaded MnO₂ and chlorine intercalated g-C₃N₄ coupling impart enhanced visible light photoactivities for pollutants degradation. *J. Photochem. Photobiol. A-Chem.* **2019**, *380*, 111867. [[CrossRef](#)]
212. Pradhan, M.R.; Rath, D.; Sethi, R.; Nanda, B.B.; Nanda, B. alpha-MnO₂ modified exfoliated porous g-C₃N₄ nanosheet (2D) for enhanced photocatalytic oxidation efficiency of aromatic alcohols. *Inorg. Chem. Commun.* **2021**, *130*, 108717. [[CrossRef](#)]
213. Dong, J.; Xie, H.; Feng, R.; Lai, X.; Duan, H.; Xu, L.; Xia, X. Transport and fate of antibiotics in a typical aqua-agricultural catchment explained by rainfall events: Implications for catchment management. *J. Environ. Manag.* **2021**, *293*, 112953. [[CrossRef](#)] [[PubMed](#)]
214. Zhao, F.; Chen, L.; Yang, L.; Sun, L.; Li, S.; Li, M.; Feng, Q. Effects of land use and rainfall on sequestration of veterinary antibiotics in soils at the hillslope scale. *Environ. Pollut.* **2020**, *260*, 114112. [[CrossRef](#)]
215. Wang, J.; Zhuan, R. Degradation of antibiotics by advanced oxidation processes: An overview. *Sci. Total Environ.* **2020**, *701*, 135023. [[CrossRef](#)] [[PubMed](#)]
216. Ahmadijokani, F.; Molavi, H.; Tajahmadi, S.; Rezakazemi, M.; Amini, M.; Kamkar, M.; Rojas, O.J.; Arjmand, M. Coordination chemistry of metal-organic frameworks: Detection, adsorption, and photodegradation of tetracycline antibiotics and beyond. *Coord. Chem. Rev.* **2022**, *464*, 214562. [[CrossRef](#)]
217. Qin, K.; Zhao, Q.; Yu, H.; Xia, X.; Li, J.; He, S.; Wei, L.; An, T. A review of bismuth-based photocatalysts for antibiotic degradation: Insight into the photocatalytic degradation performance, pathways and relevant mechanisms. *Environ. Res.* **2021**, *199*, 111360. [[CrossRef](#)]
218. Ma, W.; Xu, X.; An, B.; Zhou, K.; Mi, K.; Huo, M.; Liu, H.; Wang, H.; Liu, Z.; Cheng, G.; et al. Single and ternary competitive adsorption-desorption and degradation of amphenicol antibiotics in three agricultural soils. *J. Environ. Manag.* **2021**, *297*, 113366. [[CrossRef](#)]

219. Wahab, M.; Zahoor, M.; Salman, S.M.; Kamran, A.W.; Naz, S.; Burlakovs, J.; Kallistova, A.; Pimenov, N.; Zekker, I. Adsorption-Membrane Hybrid Approach for the Removal of Azithromycin from Water: An Attempt to Minimize Drug Resistance Problem. *Water* **2021**, *13*, 1969. [CrossRef]
220. Bai, X.; Chen, W.; Wang, B.; Sun, T.; Wu, B.; Wang, Y. Photocatalytic Degradation of Some Typical Antibiotics: Recent Advances and Future Outlooks. *Int. J. Mol. Sci.* **2022**, *23*, 8130. [CrossRef]
221. Chen, Y.; Yang, J.; Zeng, L.; Zhu, M. Recent progress on the removal of antibiotic pollutants using photocatalytic oxidation process. *Crit. Rev. Environ. Sci. Technol.* **2022**, *52*, 1401–1448. [CrossRef]
222. Wu, S.; Lin, Y.; Hu, Y.H. Strategies of tuning catalysts for efficient photodegradation of antibiotics in water environments: A review. *J. Mater. Chem. A* **2021**, *9*, 2592–2611. [CrossRef]
223. Pattanayak, D.S.; Pal, D.; Mishra, J.; Thakur, C. Noble metal-free doped graphitic carbon nitride (g-C₃N₄) for efficient photodegradation of antibiotics: Progress, limitations, and future directions. *Environ. Sci. Pollut. Res.* **2022**, 1–13. [CrossRef] [PubMed]
224. Bisaria, K.; Sinha, S.; Singh, R.; Iqbal, H.M.N. Recent advances in structural modifications of photo-catalysts for organic pollutants degradation-A comprehensive review. *Chemosphere* **2021**, *284*, 131263. [CrossRef] [PubMed]
225. Hong, X.; Li, Y.; Wang, X.; Long, J.; Liang, B. Carbon nanosheet/MnO₂/BiOCl ternary composite for degradation of organic pollutants. *J. Alloys Compd.* **2022**, *891*, 162090. [CrossRef]
226. Chen, R.R. *Preparation and Degradation of g-C₃N₄ Based Photocatalysts*; Anhui Jianzhu University: Hefei, China, 2021.
227. Du, C.; Zhang, Z.; Tan, S.; Yu, G.; Chen, H.; Zhou, L.; Yu, L.; Su, Y.; Zhang, Y.; Deng, F.; et al. Construction of Z-scheme g-CN₄/MnO₂/GO ternary photocatalyst with enhanced photodegradation ability of tetracycline hydrochloride under visible light radiation. *Environ. Res.* **2021**, *200*, 111427. [CrossRef]
228. Liu, H.; Zou, X.; Chen, Q.; Fan, W.; Gong, Z. Pumice-loaded rGO@MnO₂ nanomesh photocatalyst with visible light response for rapid degradation of ciprofloxacin. *Sep. Purif. Technol.* **2022**, *297*, 121502. [CrossRef]
229. Kaur, P.K.; Badru, R.; Singh, P.P.; Kaushal, S. Photodegradation of organic pollutants using heterojunctions: A review. *J. Environ. Chem. Eng.* **2020**, *8*, 103666. [CrossRef]
230. Natarajan, S.; Bajaj, H.C.; Tayade, R.J. Recent advances based on the synergetic effect of adsorption for removal of dyes from waste water using photocatalytic process. *J. Environ. Sci.* **2018**, *65*, 201–222. [CrossRef]
231. Badvi, K.; Javanbakht, V. Enhanced photocatalytic degradation of dye contaminants with TiO₂ immobilized on ZSM-5 zeolite modified with nickel nanoparticles. *J. Clean. Prod.* **2021**, *280*, 124518. [CrossRef]
232. Jabeen, S.; Khan, M.S.; Khattak, R.; Zekker, I.; Burlakovs, J.; Rubin, S.S.d.; Ghangrekar, M.M.; Kallistova, A.; Pimenov, N.; Zahoor, M.; et al. Palladium-Supported Zirconia-Based Catalytic Degradation of Rhodamine-B Dye from Wastewater. *Water* **2021**, *13*, 1522. [CrossRef]
233. Zangeneh, H.; Zinatizadeh, A.A.L.; Habibi, M.; Akia, M.; Isa, M.H. Photocatalytic oxidation of organic dyes and pollutants in wastewater using different modified titanium dioxides: A comparative review. *J. Ind. Eng. Chem.* **2015**, *26*, 1–36. [CrossRef]
234. Rahman, N.U.; Ullah, I.; Alam, S.; Khan, M.S.; Shah, L.A.; Zekker, I.; Burlakovs, J.; Kallistova, A.; Pimenov, N.; Vincevica-Gaile, Z.; et al. Activated Ailanthus altissima Sawdust as Adsorbent for Removal of Acid Yellow 29 from Wastewater: Kinetics Approach. *Water* **2021**, *13*, 2136. [CrossRef]
235. Gusain, R.; Gupta, K.; Joshi, P.; Khatri, O.P. Adsorptive removal and photocatalytic degradation of organic pollutants using metal oxides and their composites: A comprehensive review. *Adv. Colloid Interface Sci.* **2019**, *272*, 102009. [CrossRef] [PubMed]
236. Hitam, C.N.C.; Jalil, A.A. A review on exploration of Fe₂O₃ photocatalyst towards degradation of dyes and organic contaminants. *J. Environ. Manag.* **2020**, *258*, 110050. [CrossRef] [PubMed]
237. Hasanpour, M.; Hatami, M. Photocatalytic performance of aerogels for organic dyes removal from wastewaters: Review study. *J. Mol. Liq.* **2020**, *309*, 113094. [CrossRef]
238. Saroyan, H.; Kyzas, G.Z.; Deliyanni, E.A. Effective Dye Degradation by Graphene Oxide Supported Manganese Oxide. *Processes* **2019**, *7*, 40. [CrossRef]
239. Warsi, M.F.; Bilal, M.; Zulfiqar, S.; Khalid, M.U.; Agboola, P.O.; Shakir, I. Enhanced visible light driven Photocatalytic activity of MnO₂ nanomaterials and their hybrid structure with carbon nanotubes. *Mater. Res. Express* **2020**, *7*, 105015. [CrossRef]
240. Warsi, M.F.; Bashir, B.; Zulfiqar, S.; Aadil, M.; Khalid, M.U.; Agboola, P.O.; Shakir, I.; Yousuf, M.A.; Shahid, M. Mn_{1-x}Cu_xO₂/reduced graphene oxide nanocomposites: Synthesis, characterization, and evaluation of visible light mediated catalytic studies. *Ceram. Int.* **2021**, *47*, 5044–5053. [CrossRef]
241. Siddiqui, S.I.; Manzoor, O.; Mohsin, M.; Chaudhry, S.A. Nigella sativa seed based nanocomposite-MnO₂/BC: An antibacterial material for photocatalytic degradation, and adsorptive removal of Methylene blue from water. *Environ. Res.* **2019**, *171*, 328–340. [CrossRef]
242. Zhang, L.; Jamal, R.; Zhao, Q.; Wang, M.; Abdiryim, T. Preparation of PEDOT/GO, PEDOT/MnO₂, and PEDOT/GO/MnO₂ nanocomposites and their application in catalytic degradation of methylene blue. *Nanoscale Res. Lett.* **2015**, *10*, 1–9. [CrossRef]
243. Siddeswara, D.M.K.; Venkatesh, T.; Mahesh, K.R.V.; Mylarappa, M.; Anantharaju, K.S.; Kumara, K.N.S.; Raghavendra, N.; Shivakumar, M.S. One Step Synthesis of Ternary Composite of GNS/CNT/MnO₂ for the Applications of Electrochemical and Photocatalytic Studies. In Proceedings of the International Conference on Nanotechnology (ICNano), Karnataka, India, 21–23 April 2017; pp. 11799–11805.

244. Singh, A.K.; Gautam, R.K.; Agrahari, S.; Prajapati, J.; Tiwari, I. Graphene oxide supported Fe₃O₄-MnO₂ nanocomposites for adsorption and photocatalytic degradation of dyestuff: Ultrasound effect, surfactants role and real sample analysis. *Int. J. Environ. Anal. Chem.* **2022**, *1*, 1–27. [[CrossRef](#)]
245. Chen, R.-R.; Ren, Q.-F.; Liu, Y.-X.; Ding, Y.; Zhu, H.-T.; Xiong, C.-Y.; Jin, Z.; Oh, W.-C. Synthesis of g-C₃N₄/diatomite/MnO₂ composites and their enhanced photo-catalytic activity driven by visible light. *J. Korean Ceram. Soc.* **2021**, *58*, 548–558. [[CrossRef](#)]
246. Ahmad, J.; Wahid, M.; Majid, K. In situ construction of hybrid MnO₂@GO heterostructures for enhanced visible light photocatalytic, anti-inflammatory and anti-oxidant activity. *New J. Chem.* **2020**, *44*, 11092–11104. [[CrossRef](#)]
247. Vikal, M.; Shah, S.; Singh, N.; Singh, P.; Gupta, M.; Singh, M.J.; Kumar, A.; Kumar, Y. Efficient MnO₂ decorated graphitic carbon nitride-based nanocomposite for application in water purification. *Mater. Today Proc.* **2022**, *67*, 777–783. [[CrossRef](#)]
248. Gayathri, M.; Shanthi, M.; Satheeshkumar, E.; Jayaprakash, N.; Sundaravadivel, E. Preparation and characterization of boron doped CN's/MnO₂ and its photocatalytic application of dye degradation. In Proceedings of the 2nd International Conference on Recent Advances in Materials and Manufacturing (ICRAMM), Tamil Nadu, India, 20–21 November 2021; pp. 1506–1512.
249. Ma, M.; Yang, Y.; Chen, Y.; Jiang, J.; Ma, Y.; Wang, Z.; Huang, W.; Wang, S.; Liu, M.; Ma, D.; et al. Fabrication of hollow flower-like magnetic Fe₃O₄/C/MnO₂/C₃N₄ composite with enhanced photocatalytic activity. *Sci. Rep.* **2021**, *11*, 1–10. [[CrossRef](#)] [[PubMed](#)]
250. Park, Y.; Numan, A.; Ponomarev, N.; Iqbal, J.; Khalid, M. Enhanced photocatalytic performance of PANI-rGO-MnO₂ ternary composite for degradation of organic contaminants under visible light. *J. Environ. Chem. Eng.* **2021**, *9*, 106006. [[CrossRef](#)]
251. Panimalar, S.; Uthrakumar, R.; Selvi, E.T.; Gomathy, P.; Inmozhi, C.; Kaviyarasu, K.; Kennedy, J. Studies of MnO₂/g-C₃N₄ hetrostructure efficient of visible light photocatalyst for pollutants degradation by sol-gel technique. *Surf. Interfaces* **2020**, *20*, 100512. [[CrossRef](#)]
252. Tahir, M.B.; Kiran, H.; Iqbal, T. The detoxification of heavy metals from aqueous environment using nano-photocatalysis approach: A review. *Environ. Sci. Pollut. Res.* **2019**, *26*, 10515–10528. [[CrossRef](#)]
253. Barakat, M.A. New trends in removing heavy metals from industrial wastewater. *Arab. J. Chem.* **2011**, *4*, 361–377. [[CrossRef](#)]
254. Bashir, A.; Malik, L.A.; Ahad, S.; Manzoor, T.; Bhat, M.A.; Dar, G.N.; Pandith, A.H. Removal of heavy metal ions from aqueous system by ion-exchange and biosorption methods. *Environ. Chem. Lett.* **2019**, *17*, 729–754. [[CrossRef](#)]
255. Fadlalla, M.I.; Kumar, P.S.; Selvam, V.; Babu, S.G. Emerging energy and environmental application of graphene and their composites: A review. *J. Mater. Sci.* **2020**, *55*, 7156–7183. [[CrossRef](#)]
256. Zhang, L.; Tian, Y.; Guo, Y.; Gao, H.; Li, H.; Yan, S. Introduction of alpha-MnO₂ nanosheets to NH₂ graphene to remove Cr⁶⁺ from aqueous solutions. *RSC Adv.* **2015**, *5*, 44096–44106. [[CrossRef](#)]
257. Li, Z.; Wang, L.; Qin, L.; Lai, C.; Wang, Z.; Zhou, M.; Xiao, L.; Liu, S.; Zhang, M. Recent advances in the application of water-stable metal-organic frameworks: Adsorption and photocatalytic reduction of heavy metal in water. *Chemosphere* **2021**, *285*, 131432. [[CrossRef](#)] [[PubMed](#)]
258. Kumar, V.; Singh, V.; Kim, K.-H.; Kwon, E.E.; Younis, S.A. Metal-organic frameworks for photocatalytic detoxification of chromium and uranium in water. *Coord. Chem. Rev.* **2021**, *447*, 214148. [[CrossRef](#)]
259. Jafarzadeh, M. Recent Progress in the Development of MOF-Based Photocatalysts for the Photoreduction of Cr(VI). *ACS Appl. Mater. Interfaces* **2022**, *14*, 24993–25024. [[CrossRef](#)]
260. Padhi, D.K.; Baral, A.; Parida, K.; Singh, S.K.; Ghosh, M.K. Visible Light Active Single-Crystal Nanorod/Needle-like alpha-MnO₂@RGO Nanocomposites for Efficient Photoreduction of Cr(VI). *J. Phys. Chem. C* **2017**, *121*, 6039–6049. [[CrossRef](#)]
261. Wang, C.Y.; Chen, L.; Xu, L.; Xie, Z.J.; Liu, Y.H. Preparation of MnO₂@g-C₃N₄ and Its Photoreduction Performance for Uranium (VI). *Hydrometall. China* **2021**, *40*, 148–154. [[CrossRef](#)]

Disclaimer/Publisher's Note: The statements, opinions and data contained in all publications are solely those of the individual author(s) and contributor(s) and not of MDPI and/or the editor(s). MDPI and/or the editor(s) disclaim responsibility for any injury to people or property resulting from any ideas, methods, instructions or products referred to in the content.